DØ Note 3544
Version 2.0

W Boson Mass Measurement from Run 1b Data using Forward Detectors

Ashutosh V. Kotwal
Columbia University

Yaroslav Kulik
SUNY - Stony Brook

February 21, 1999

1 Introduction

We present a measurement of the W mass using the forward detectors and Run 1b data. We refer to many of the techniques used for the analyses using the central detector with Run 1b [1] and Run 1a [2] data.

2 Event Selection

We use the electron energy measured with the 5x5 window in the CC and the 20 cm radius cone in the EC. The recoil is computed by summing over all calorimeter cells excluding the electron cells. We use the electron cluster centroid and track centroid to measure the electron direction and define the event vertex. For the Z's, we require at least one electron to have an associated track, and the forward electron to always have an associated track. For events in which both electrons have tracks, we use the average z_{vtx} (for CC-CC Z's) or z_{vtx} defined by the more central electron (CC-EC and EC-EC Z's).

We select central electrons by requiring:

- EM fraction > 0.9
- H-matrix $\chi^2 < 100$
- track match significance < 5
- electron isolation < 0.15
- $\mid Z_{clus} \mid < 108$ cm
- $\mid Z_{trk} \mid < 80$ cm
- 10% ϕ cut on either side of CC module edge

We select forward electrons by requiring:

- EM fraction > 0.9
- H-matrix $\chi^2 < 200$
- track match significance < 10
- electron isolation < 0.15
- 4-variable likelihood ratio $\lambda_4 < 4.0$
- $1.5 < \eta_{det} < 2.5$

We select the W sample by requiring:

- RECO versions in the range [12.13,12.25]
- EM1_EISTRKCC_MS trigger
- neither MICRO_BLANK nor MRBS_LOSS conditions should be true
- $p_t(e) > 25$ GeV (CC) or $p_t(e) > 30$ GeV (EC)
- $p_t(\nu) > 25$ GeV (CC) or $p_t(\nu) > 30$ GeV (EC)
- $p_t(W) < 15$ GeV
- $\mid Z_{vtx} \mid < 100$ cm

We select the Z sample by requiring

- RECO versions in the range [12.13,12.25]
- EM2_EIS2_HI trigger
- two electrons with $p_t^e > 25$ GeV (CC) or $p_t^e > 30$ GeV (EC)
- $60 < m_{ee} < 120$ GeV
- $\mid Z_{vtx} \mid < 100$ cm
- at least one electron has a track, and a forward electron always has a track.

A standard bad run list [1] is used to exclude certain runs from the data sample. The number of W and Z candidates in the various topologies is shown in table 1.

Table 1: Number of W and Z candidate events.

	CC W	EC W	CC-CC Z	CC-EC Z	EC-EC Z
Events	28420	11090	2091	1265	422

3 Production Model

We modify the production model used for the CC W mass analysis in the CMS Monte Carlo in the following respect. The CMS Monte Carlo [3, 4] is a fast event generator combined with a parametric detector simulation, used in the published Run 1b analysis [1] of the W mass using central W's only. We extend the applicability of this Monte Carlo program for the W mass measurement using forward W's and use it as described in the following.

The parton luminosity parameter β is computed and used separately for the two W topologies (CC electron and EC electron) and the three Z topologies (CC-CC, CC-EC, EC-EC). We use HERWIG and the MRSA$'$ pdf's to

[1] kindly provided by Eric Flattum.

generate $W \to e\nu$ and $Z \to ee$ events. We define a CC electron by $\eta_e < 1.0$ and an EC electron by $1.5 < \eta_e < 2.5$. W and Z events are classified according to the electron topologies. We fit the mass distribution in each category with the appropriate Breit-Wigner line shape skewed by the parton luminosity factor, where β and the overall normalization are the free parameters. The results of the fits are shown in figures 1 and 2.

We compute the sea-sea fraction of the W events as the fraction of the HERWIG events generated from two sea quarks. We obtain $f_{ss} = (18.99 \pm 0.57)$ % for EC W's and $f_{ss} = (19.83 \pm 0.39)$ % for CC W's, where the uncertainties are statistical. Within statistical errors f_{ss} is the same for CC and EC W's.

4 Alignment and Position Calibration

In this analysis, the radial position of the FDC track centroid sets the angular scale for the forward detectors. The transverse alignment of the FDC's is performed by minimizing the beam impact parameter of electrons from the W sample [5]. We use collider data to cross-check the test beam calibration of the FDC. Using the muon system as reference, the radial scale of the FDC is checked with a sample of inclusive forward muons. The second reference point is obtained from reconstructed vertex, which is calibrated using a sample of inclusive central muons.

In order to calibrate the z coordinate of the reconstructed vertex, we extrapolate the line obtained by connecting the muon A layer hit and the CDC track centroid to the beam axis. The CDC track centroid has been corrected for the z bias [6] by scaling with the factor of 0.988. The residue between the reconstructed vertex z position and the predicted muon position at the beam axis is plotted in bins of the vertex position. The residue distribution is fitted with the sum of two Gaussians to allow for background. The mean of the signal Gaussian is plotted as a function of the z position of the vertex in order to measure any bias. The bias is shown in figure 3. We find that a scale factor correction

$$Z_{vtx} \to Z_{vtx} \times 0.9827 \tag{1}$$

makes the reconstructed vertex position consistent with the predicted muon position, as shown in figure 4.

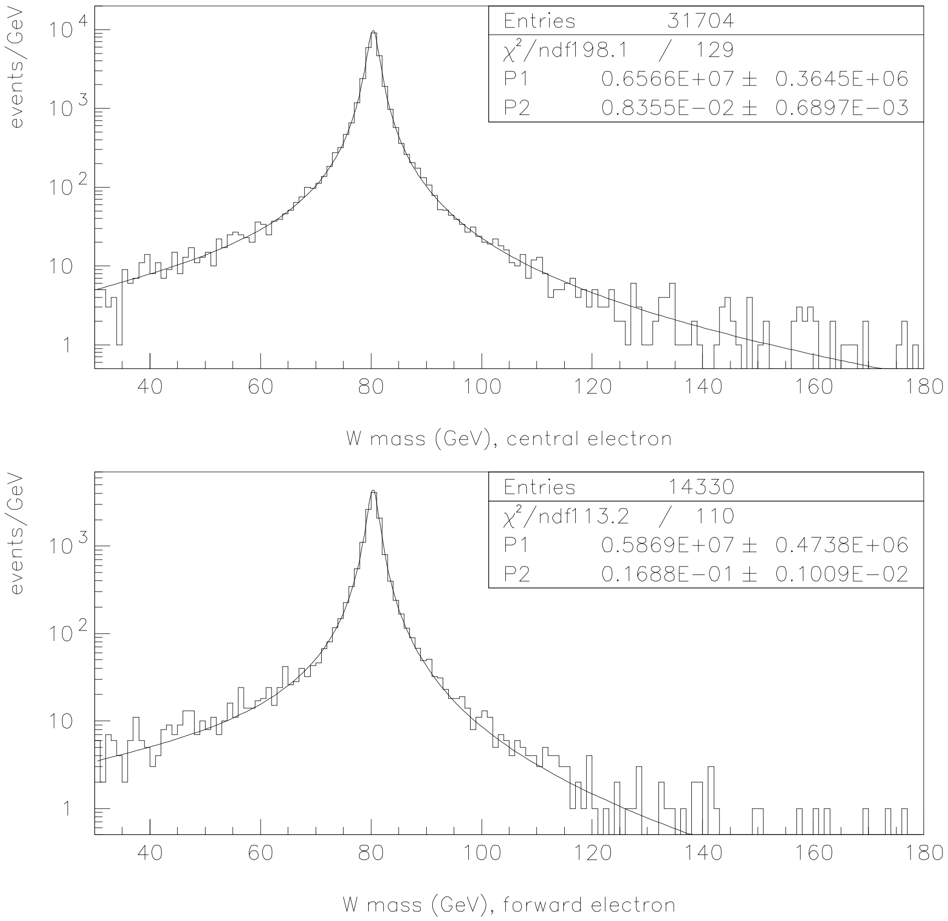

Figure 1: Mass distributions of HERWIG $W \to e\nu$ events, fitted for the parton luminosity parameter β, given by P_2.

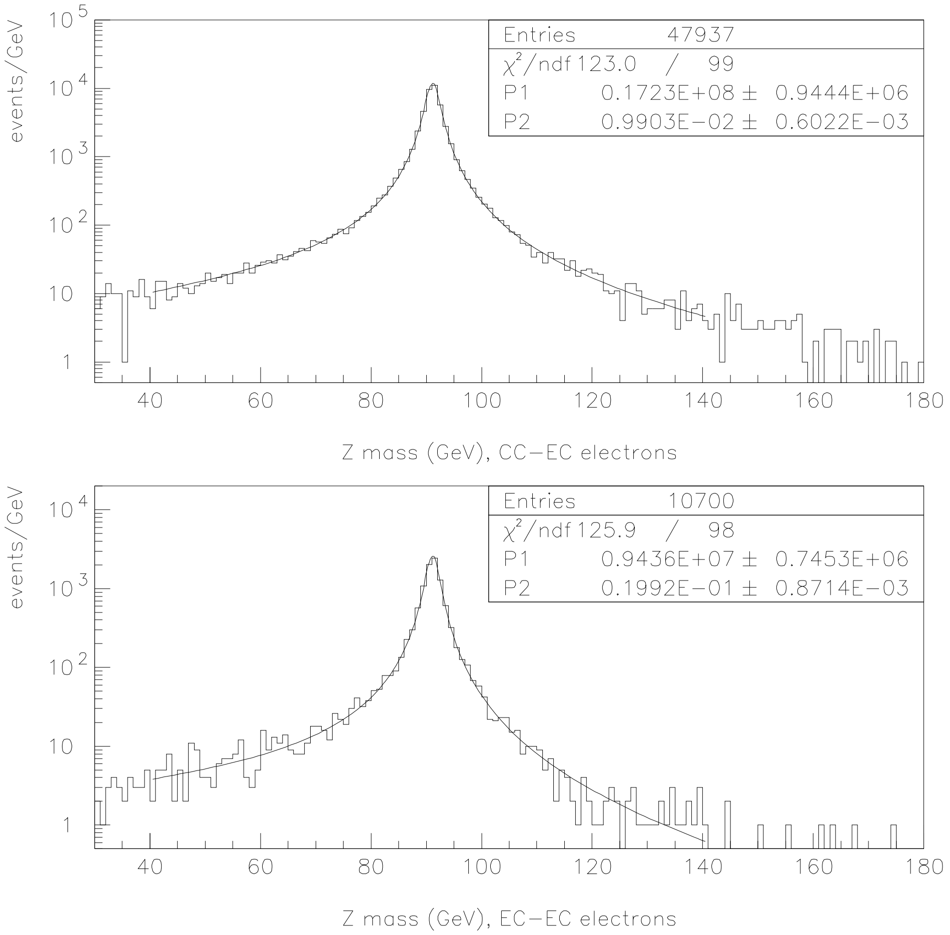

Figure 2: Mass distributions of HERWIG $Z \to ee$ events, fitted for the parton luminosity parameter β, given by P_2.

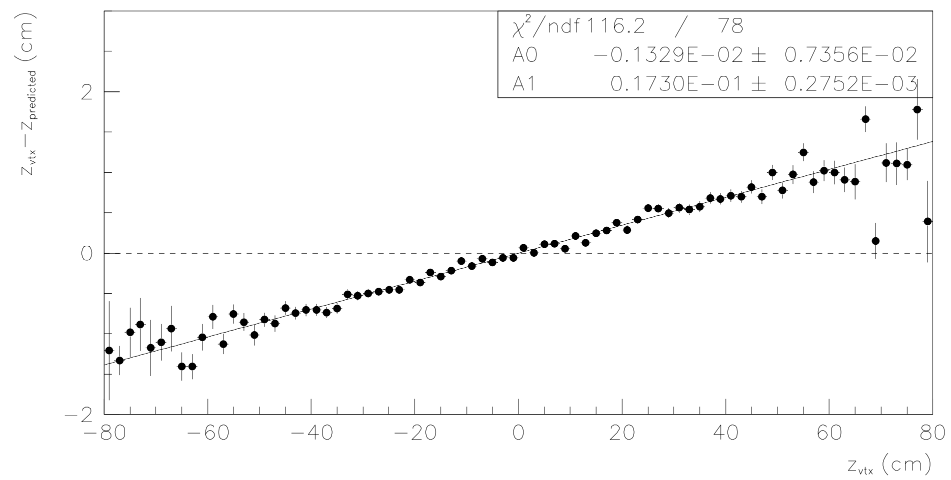

Figure 3: Residue of the z position of the reconstructed vertex from the z position of central muon tracks at the beam, as a function of the vertex z position. The solid line is a fitted straight line and the dashed line is $\Delta z = 0$.

Using the corrected z position of the reconstructed vertex and the A layer hit position of the forward muon system, the predicted FDC centroid radius is compared to the measured FDC track centroid, in bins of FDC centroid radius. Double Gaussian fits to the residue distributions are used to extract the FDC radial calibration taking into account the background. The radial residue as a function of the radius is shown in figure 5. The slope of the proportionality line is consistent with zero, indicating that no re-calibration of the FDC radial coordinate is needed.

The EC's are aligned in the transverse directions with respect to the FDC's using the electrons from the W sample [7]. The radial position of the EC cluster is calibrated against the FDC track centroid using the electron pairs from the CC-EC Z sample, where the vertex is defined by the CC electron [8]. The χ^2 as a function of the EC radial scale is shown in figure 6. The radial coordinate of the EC cluster centroid is corrected according to

$$\begin{aligned} R_{clus}^{ECN} &\rightarrow R_{clus}^{ECN}/(0.9997 \pm 0.00044) \\ R_{clus}^{ECS} &\rightarrow R_{clus}^{ECS}/(1.00225 \pm 0.00044) \end{aligned} \quad (2)$$

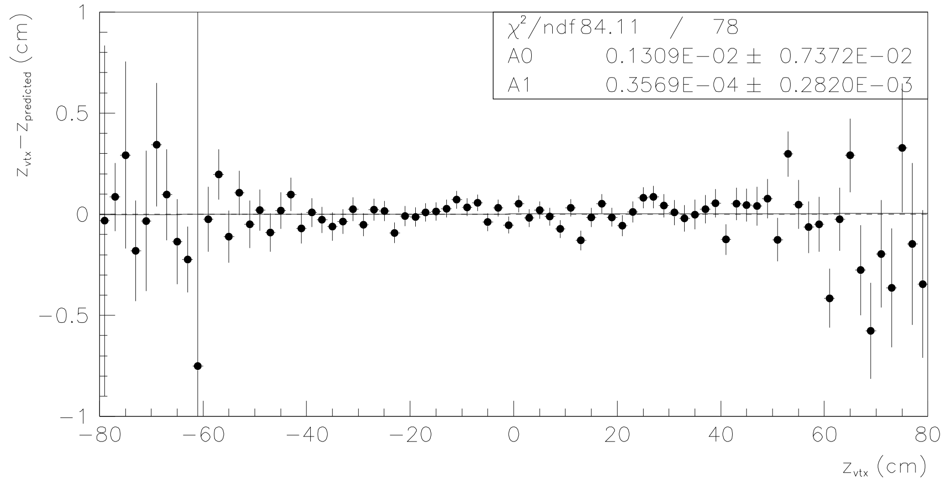

Figure 4: Residue of the z position of the corrected reconstructed vertex from the z position of central muon tracks at the beam, as a function of the vertex z position. The solid line is a fitted straight line and the dashed line is $\Delta z = 0$.

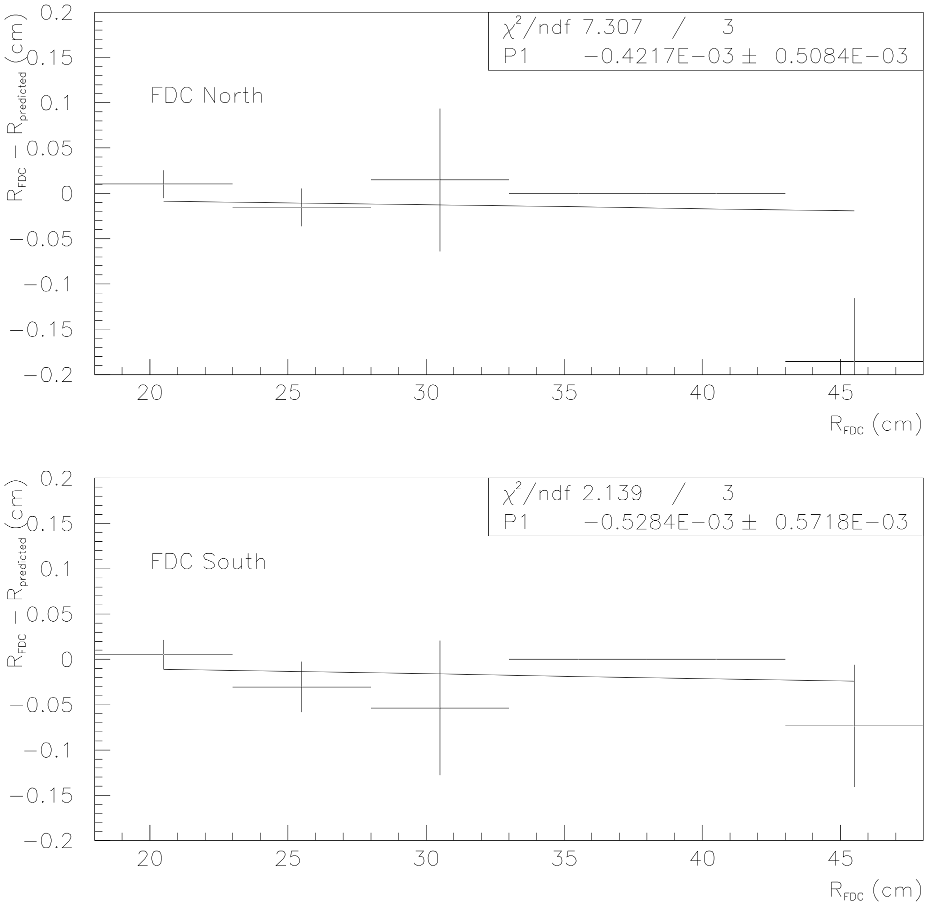

Figure 5: Residue of the radial position of the FDC track centroid from the predicted radial position of forward muon tracks at the FDC, as a function of the track radial position. The solid line is a fitted proportionality line.

which is tantamount to shifts in the z direction.

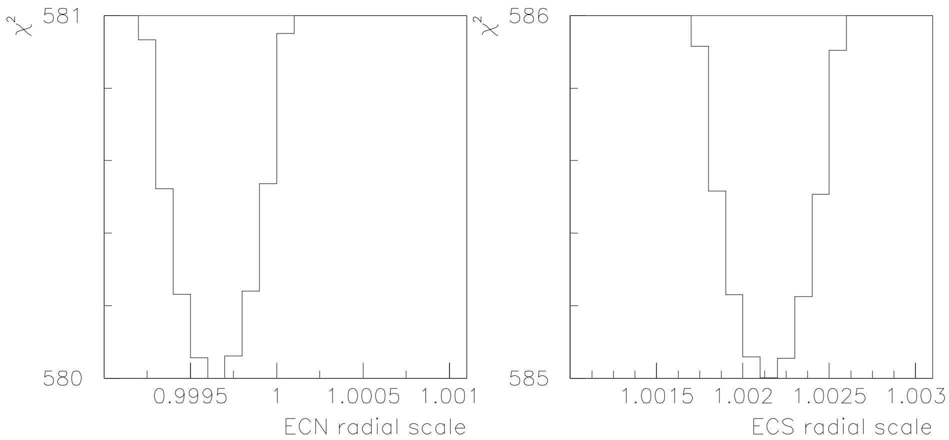

Figure 6: χ^2 of $z_1 - z_2$ using CC-EC Z events, as a function of the EC radial scale.

5 Underlying Event Correction to Electron and Recoil

As discussed in [9], the underlying event contribution to the electron energy is measured from the W events using rotated electron cones of radius 20 cm.

Figure 7 shows the luminosity dependence of the underlying event correction to the recoil E_T, due to the electron overlap. The $U_{||}$ correction is normalized to the $\eta\phi$ area of the cone. The same measurement performed with the 5x5 window is shown for comparison. We find consistent results with the two algorithms.

We use the measured slope from figure 7 to extrapolate the $U_{||}$ correction to $\mathcal{L} = 0$. The $\mid \eta \mid$ dependence of the $U_{||}$ correction at $\mathcal{L} = 0$ is shown in figure 8, along with the fitted cubic polynomial in $(\mid \eta \mid -2.0)$.

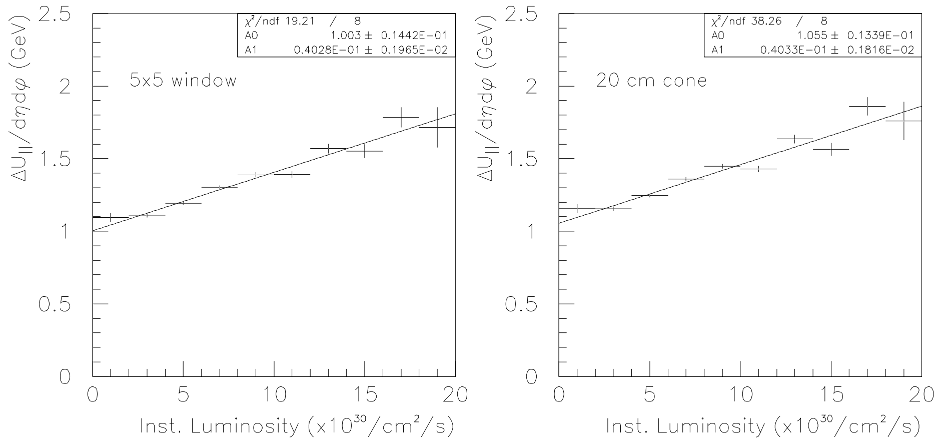

Figure 7: Luminosity dependence of the correction to the recoil E_T due to the electron overlap.

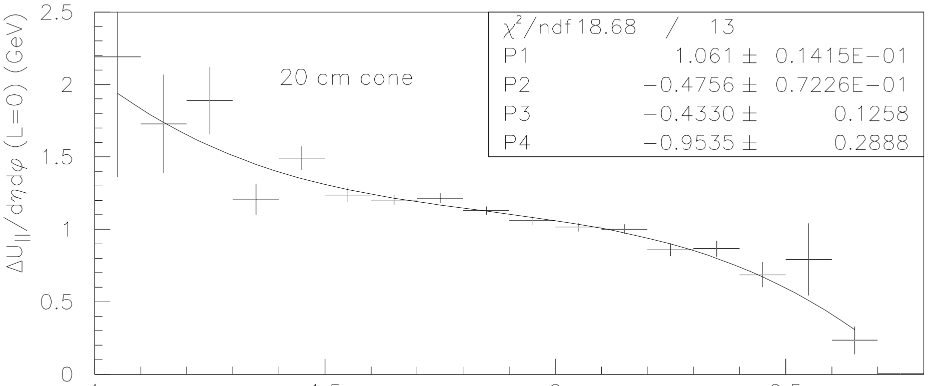

Figure 8: η dependence of the $U_{||}$ correction at $\mathcal{L} = 0$. The fit is a cubic polynomial in $(\mid \eta \mid -2.0)$.

We study the $U_{||}$ dependence of the $U_{||}$ correction at $\mathcal{L} = 0, \mid \eta \mid= 2.0$. The dependence is fitted with a sixth order polynomial, as shown in figure 9. For this fit we relax the p_t^W cut to $p_t^W < 30$ GeV.

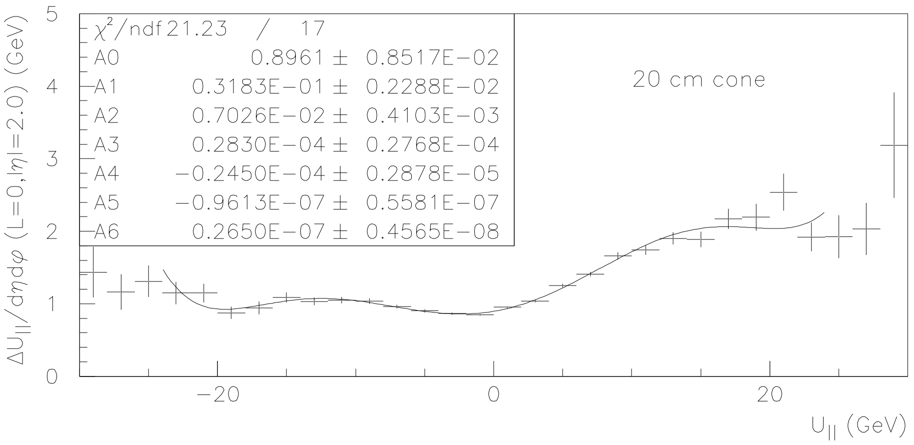

Figure 9: $U_{||}$ dependence of the $U_{||}$ correction at $\mathcal{L} = 0, \mid \eta \mid= 2.0$. The fit is to a sixth-order polynomial.

The distribution of the $U_{||}$ correction, after removing the luminosity, η and $U_{||}$ dependence is shown in figure 10. This distribution is used to simulate the resolution on the correction in the CMS Monte Carlo.

Since the algorithms for computing the electron E_T and recoil E_T are different, the underlying event correction to the electron and recoil can be different. We plot the electron correction against the recoil correction in η bins and fit the same with a proportionality factor. The fitted proportionality factor is plotted as a function of $\mid \eta \mid$ in figure 11. This dependence is fitted to a parabola, and is used to scale the $U_{||}$ correction discussed above to obtain the correction to the electron E_T.

The fluctuations in the electron E_T correction at a fixed value of the recoil E_T correction are characterized as a Gaussian σ, which is shown as a function of the recoil correction in figure 12. The straight line fit is used to simulate an additional source of smearing of the electron E_T as a function of the absolute value of the recoil correction.

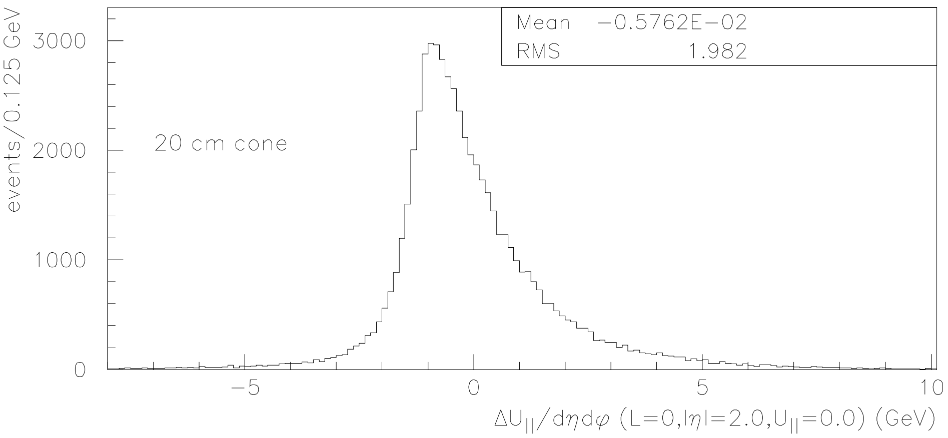

Figure 10: Distribution of the $U_{||}$ correction at $\mathcal{L} = 0, \mid \eta \mid = 2.0, U_{||} = 0.0$.

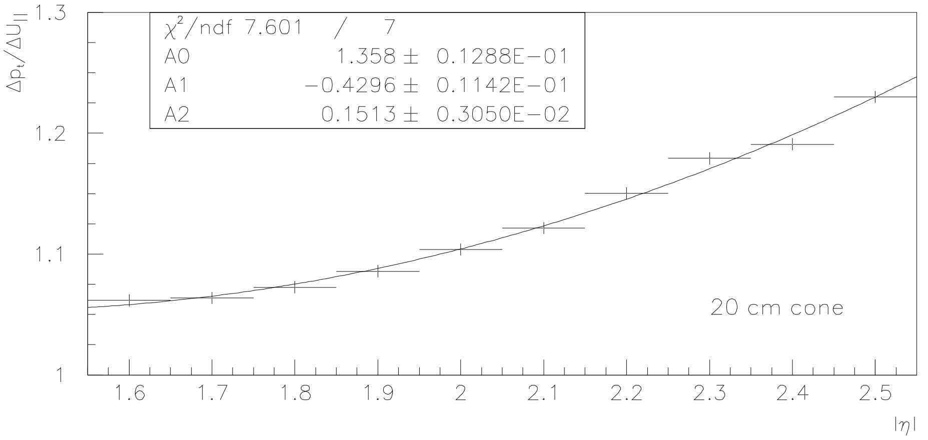

Figure 11: η dependence of the ratio of the electron E_T correction to the recoil E_T correction.

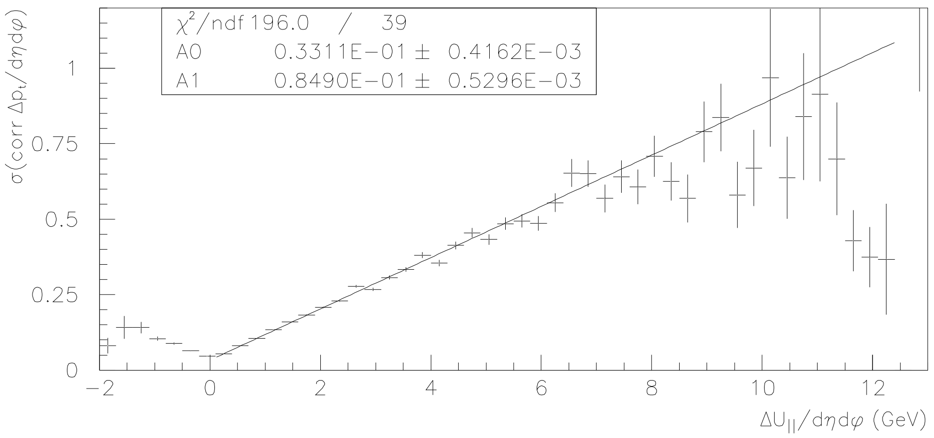

Figure 12: The spread in the electron E_T correction for different values of the recoil E_T correction.

6 Trigger Efficiencies

The electron trigger efficiency is mapped as a function of electron E_T using the EM2_EIS_EIS trigger and CC-EC Z events. The central electron is required to pass the $E_T > 20$ GeV L2 requirement, allowing the forward electron passing $E_T > 16$ GeV at L2 to measure the efficiency of the $E_T > 20$ GeV L2 cut. The measurement of the electron trigger turnon curve is documented in [10]. The EC electron trigger is fully efficient for $p_t(e) > 30$ GeV.

The $\not\!\!E_t$ trigger efficiency is measured using the following monitor triggers: EM1_ELE_MON, EM1_ELETRK_MON, ELE_1_MON and ELETRK_1_MON. These triggers are identical to the EC W signal trigger except the $\not\!\!E_t$ and the electron isolation requirements are not imposed at L2. We impose the L2 isolation condition offline. The $\not\!\!E_t$ trigger turnon efficiency is defined by the fraction of the monitor triggers which also fire the signal trigger. The measured turnon curve and the fitted parametrization used in the CMS Monte Carlo is shown in figure 13.

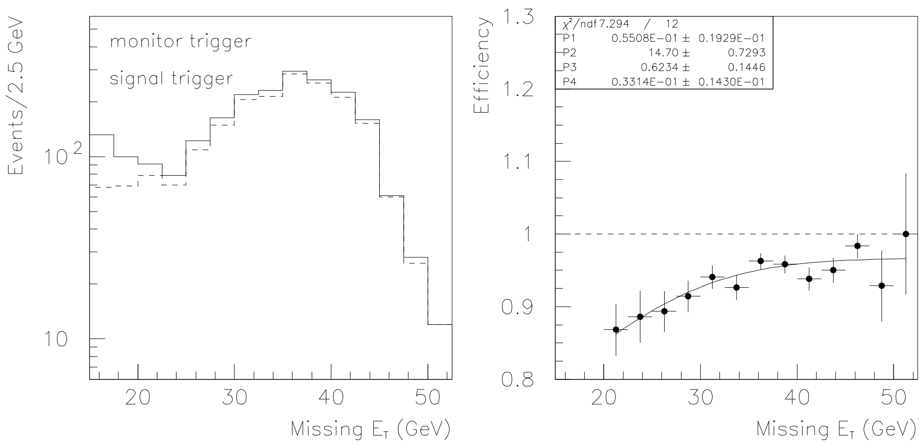

Figure 13: The efficiency of the L2 $\not{E}_t$ requirement, with the fit used in the simulation.

7 Backgrounds

We measure the fraction and shape of the QCD background in the W sample by using anti-electron cuts, and derive the normalization of the anti-electron sample from the QCD control sample at low $\not{E}_t$. The anti-electron cuts and the normalization are discussed in [11]. From the QCD control sample we measure

$$R_{norm} = 1.61 \pm 0.13 \tag{3}$$

where the uncertainty includes the difference between the measurements for EC North and EC South [11]. From the signal sample we measure

$$\begin{aligned} R_{signal} &\equiv \frac{\text{number of bad electrons}}{\text{number of good electrons}} \\ &= \frac{375}{10987} = (3.41 \pm 0.18)\% \end{aligned} \tag{4}$$

The signal sample used here (with $\not{E}_t > 30$ GeV) is different from the one used in [11], where $\not{E}_t > 25$ cut was used. We subtract the $(1.15 \pm 0.42)\%$

contamination due to good electrons in the anti-electron sample [11] to obtain

$$R_{signal} = (2.26 \pm 0.47)\% \tag{5}$$

The QCD background fraction is then given by

$$\begin{aligned} f_{QCD} &= R_{norm} \times R_{signal} \\ &= (3.64 \pm 0.78)\% \end{aligned} \tag{6}$$

We fit the anti-electron sample to extract the shape of the QCD background distribution in m_t, $E_T(e)$ and $E_T(\nu)$, after subtracting the good electron contamination. The m_t distribution is fitted with the form $P_1 \cdot (x - 60) \cdot e^{(70-x)/P_2}$, the p_t^e distribution is fitted with the form $P_1 \cdot (x - 24.5) \cdot e^{(35-x)/P_2}$, and the p_t^ν distribution is fitted with an exponential. The distributions and the fits are shown in figure 14.

We determine the shape of the QCD background in the dielectron invariant mass spectrum by making anti-electron cuts (isolation < 0.15, EM fraction > 0.9, $\chi^2 > 100$, $\sigma_{trk} < 30$) on a $Z \to ee$ candidate sample obtained using the EM2_EIS_ESC trigger. We fit the distribution in the CC-CC sample with an exponential and the CC-EC and CC-EC distributions with 4^{th} order polynomials. We fix the normalization of the Z background by fitting the invariant mass spectra with the sum of a Breit-Wigner convoluted with a Gaussian, and the background shape with its normalization floated (parameter P_4 in figure 16.) By normalizing the integral of the background shape to the total number of events, we obtain

$$\begin{aligned} f_{QCD}^{cc-cc} &= 0.0622 \pm 0.0075 \\ f_{QCD}^{cc-ec} &= 0.135 \pm 0.021 \\ f_{QCD}^{ec-ec} &= 0.128 \pm 0.022 \end{aligned} \tag{7}$$

in the mass range $60 < m_{ee} < 120$ GeV.

Backgrounds in the W sample from $Z \to ee$ where one of the electrons is lost or misreconstructed is estimated from a sample of HERWIG+SHOWERLIB Monte Carlo events. We make W and Z selection cuts on the Monte Carlo events, and normalize the number of events passing the W cuts to the number of W data events, scaled by the ratio of selected Z data and Monte Carlo events. We obtain

$$\begin{aligned} f_Z^{cc} &= 0.0033 \pm 0.0002 \\ f_Z^{ec} &= 0.0026 \pm 0.0002 \end{aligned} \tag{8}$$

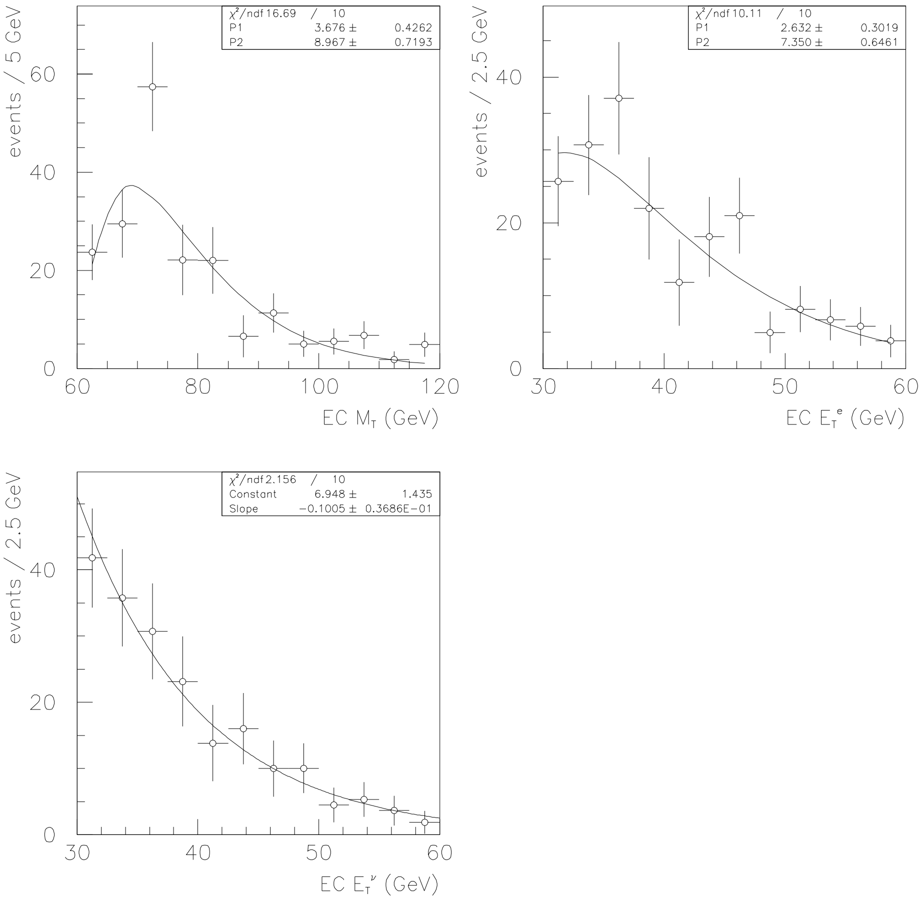

Figure 14: Fits to the m_t, p_t^e and p_t^ν distributions of events passing anti-electron cuts, representing the QCD background in the W sample.

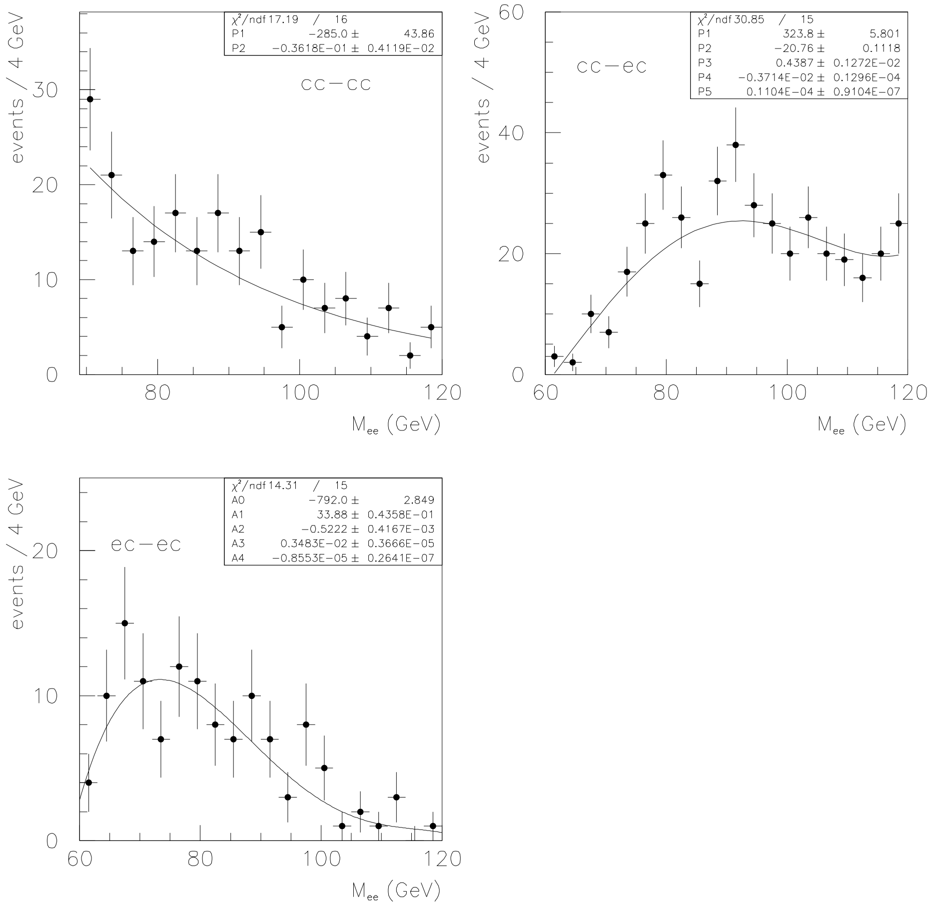

Figure 15: Fits to the dielectron invariant mass distributions of events passing anti-electron cuts, representing the QCD background in the Z sample.

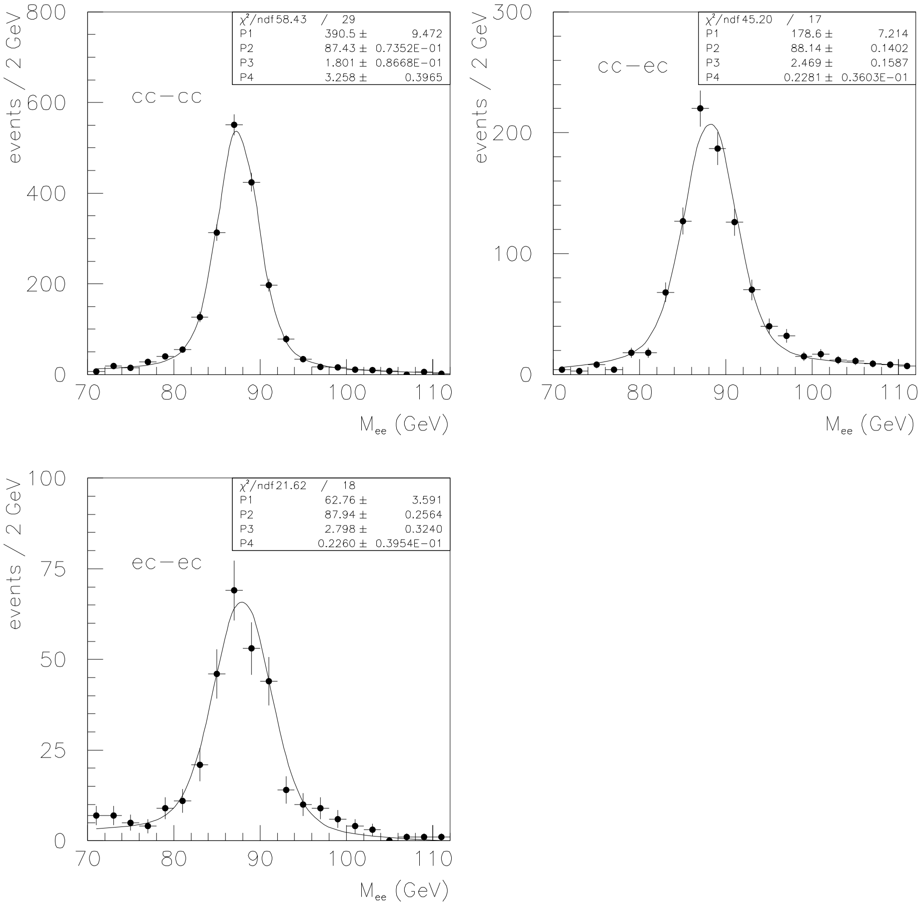

Figure 16: Fits to the dielectron invariant mass distributions with a sum of signal and background components.

where the uncertainty includes the statistical error on the MC and the uncertainty on the EM and hadronic energy scales. The m_t, p_t^e and p_t^ν distributions of the Z Monte Carlo events passing W cuts are smoothed and used to provide the shape of this background.

8 Electron Resolutions

8.1 Electron Angular Resolution

The electron angular resolution depends on the position resolution of the calorimeter cluster centroid and the track centroid. Based on the study of a plate-level GEANT $W \to e\nu$ sample overlapped with zero-bias data [12], the calorimeter cluster position resolution is set to 1 mm in the radial and ϕ directions. The FDC centroid resolution is modelled with a double Gaussian to match the distribution of the distance between the two electron vertices in $Z \to ee$ events (70 GeV $< m_{ee} <$ 100 GeV). A double Gaussian model is motivated by the presence of two kinds of FDC tracks: tracks with hits from all three FDC chambers (three segment tracks), and tracks with hits from two chambers (two segment tracks). With a narrow Gaussian resolution of 2 mm, a wide Gaussian resolution of 1.7 cm and 20% tracks in the wide Gaussian, the Monte Carlo reproduces the $z_1 - z_2$ distribution of the data (figures 17 and 18).

8.2 Electron Energy Resolution

The fractional electron energy resolution is parametrized as

$$\begin{aligned}
\sigma_E/E &= 0.13/\sqrt{E_T} \oplus\ c_{CCEM} \oplus\ N_{CC}/E\ (CC) \\
\sigma_E/E &= 0.157/\sqrt{E} \oplus\ c_{ECEM} \oplus\ N_{EC}/E\ (EC) \qquad (9)
\end{aligned}$$

where N is the noise contribution. The noise contribution is included in the distribution of the underlying event correction. The constant term is tuned by matching the observed width of the Z mass peak in the data with the Monte Carlo. The Z invariant mass spectrum is fitted with the Breit-Wigner $\oplus$ Gaussian + Background shape, shown for the data in figure 19 (P_3 is the width). For the data, we obtain

$$\sigma_m = 1.75\ \pm\ 0.08\ \text{GeV}\ (CC - CC)$$

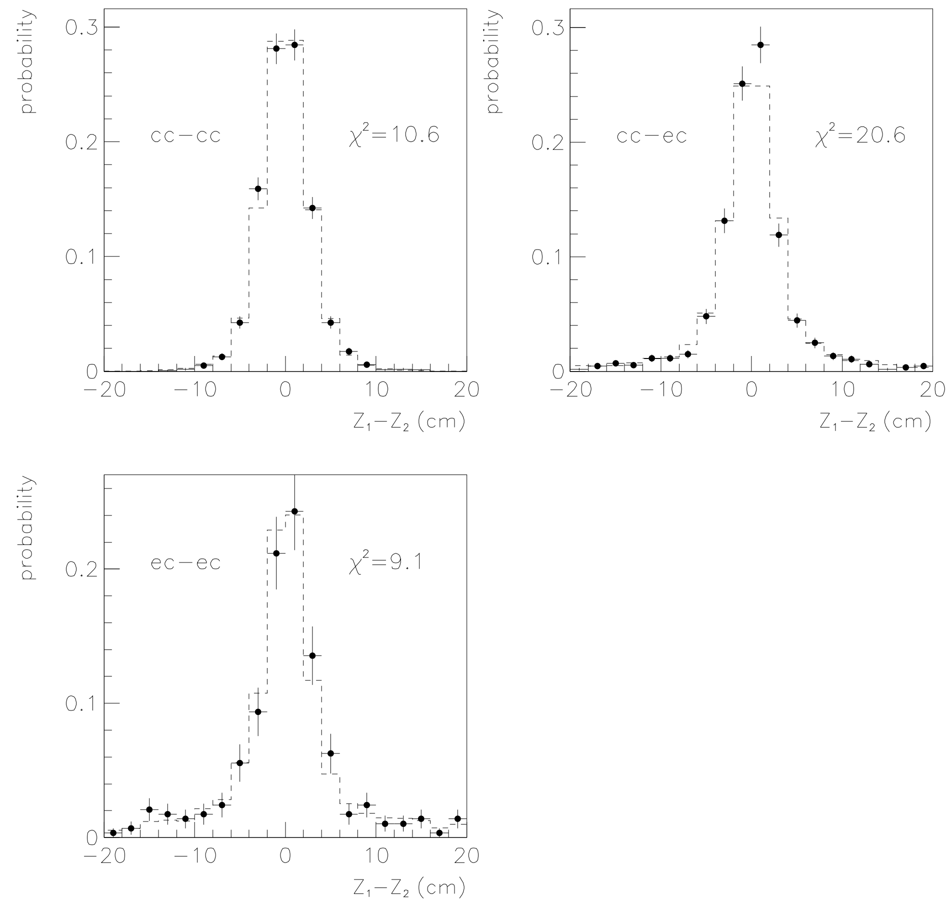

Figure 17: Difference in the positions of the electron vertices for $Z \to ee$ events, compared for data (solid points) and CMS Monte Carlo (dashed histogram).

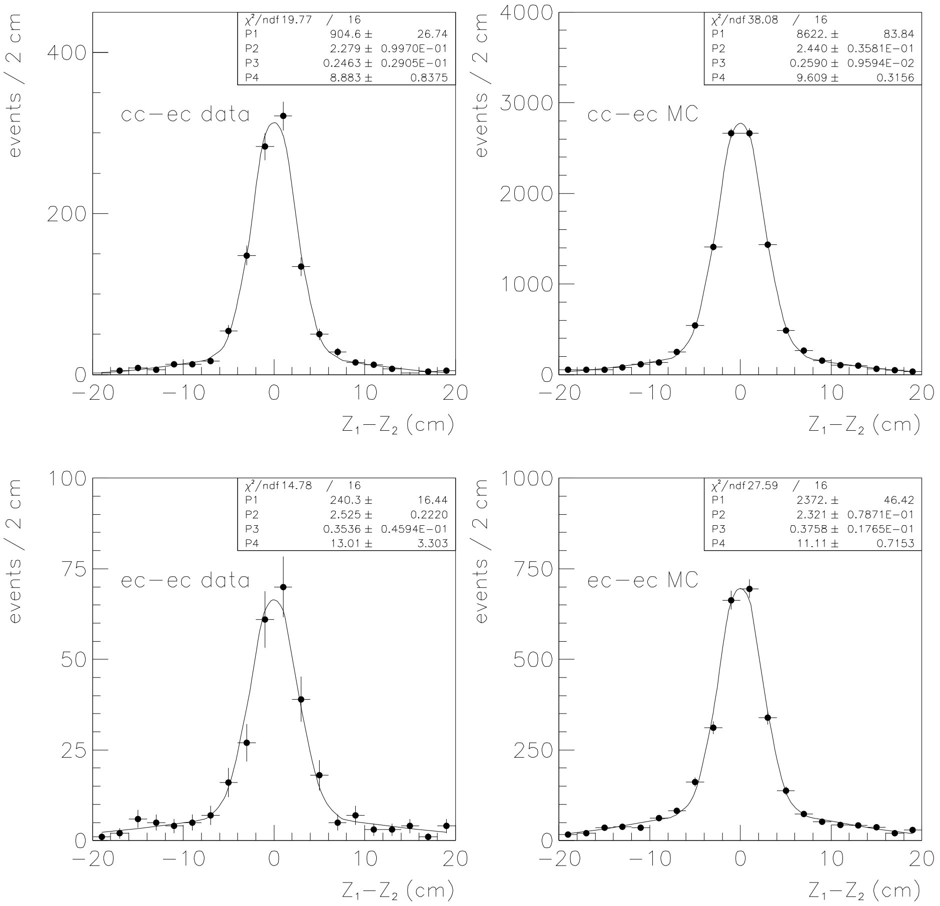

Figure 18: Difference in the positions of the electron vertices for $Z \to ee$ events, for data (left) and CMS Monte Carlo (right). The fit parameters P_2 and P_4 are the widths of two Gaussians and P_3 is the fractional area of the second Gaussian.

$$\sigma_m = 2.49 \pm 0.14 \text{ GeV } (CC - EC)$$
$$\sigma_m = 2.50 \pm 0.27 \text{ GeV } (EC - EC) \quad (10)$$

From the Monte Carlo, for a CC constant term $c_{CCEM} = 0.0115$ and an EC constant term $c_{ECEM} = 0.01$ we obtain

$$\sigma_m = 1.76 \pm 0.04 \text{ GeV } (CC - CC)$$
$$\sigma_m = 2.47 \pm 0.05 \text{ GeV } (CC - EC)$$
$$\sigma_m = 2.72 \pm 0.11 \text{ GeV } (EC - EC) \quad (11)$$

Figures 21 and 22 show the Monte Carlo predictions for the observed width of the Gaussian fitted to the Z peak as a function of the EC constant term. From the CC-EC Z events we extract $c_{ECEM} = 1.6^{+0.8}_{-1.6}$ % and from the EC-EC Z events we extract $c_{ECEM} = 0.0^{+1.0}$ %. We take the combined measurement to be

$$c_{ECEM} = 1.0^{+0.6}_{-1.0} \% \quad (12)$$

9 Recoil Measurement

9.1 Recoil Response

The recoil response is calibrated against the electron response by requiring p_t balance in $Z \to ee$ decays. The Z p_t measured with the electrons and the recoil are projected on the η axis, defined as the bisector of the two electron directions in the transverse plane. As a check of the recoil response measured with Z events of different topologies, we scale the recoil measurement with the inverse of the response parametrization

$$R_{rec} = 0.693 + 0.04 \cdot ln\ (p_t^{ee}/\text{GeV}) \quad (13)$$

and plot the sum of the projections vs p_η^{ee}, as shown in figure 23. We see minimal p_η^{ee} dependence to the p_η balance measured using the Z events with at least one central electron, which is consistent with the recoil response parametrization given above. The EC-EC Z events give a recoil response measurement statistically consistent with the above. Hence we use the same recoil response for the EC W events as for the CC W events.

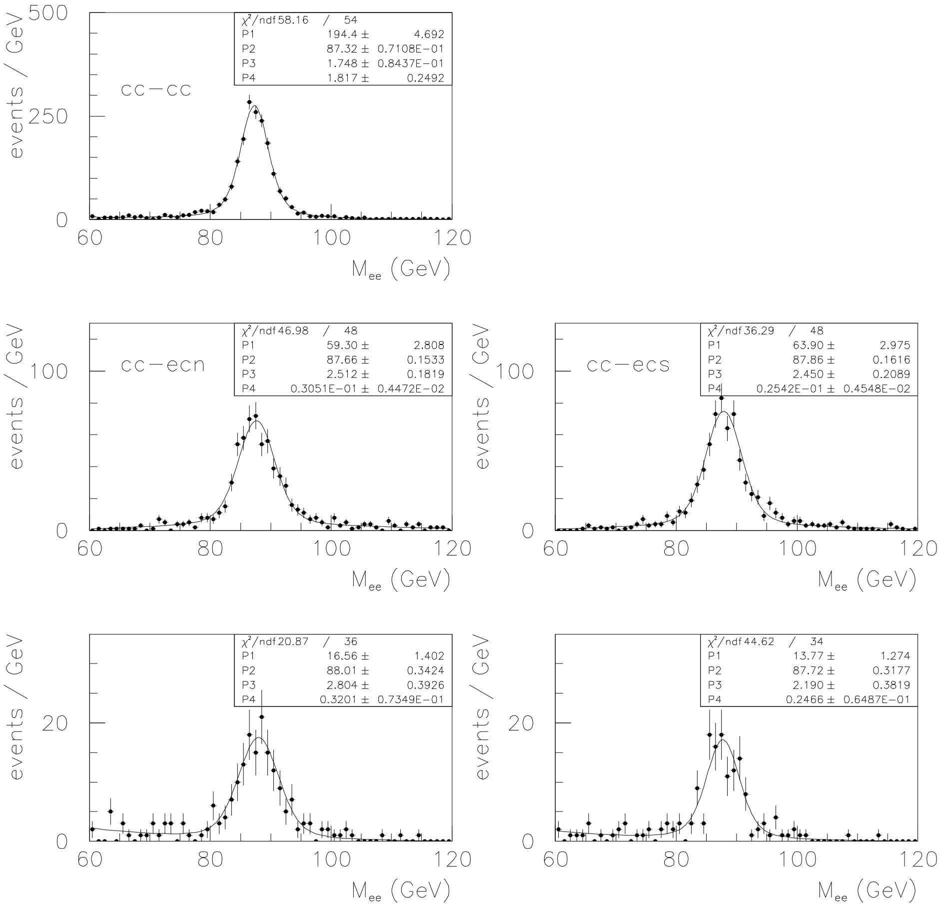

Figure 19: Fits to data to measure the Z width (P_3).

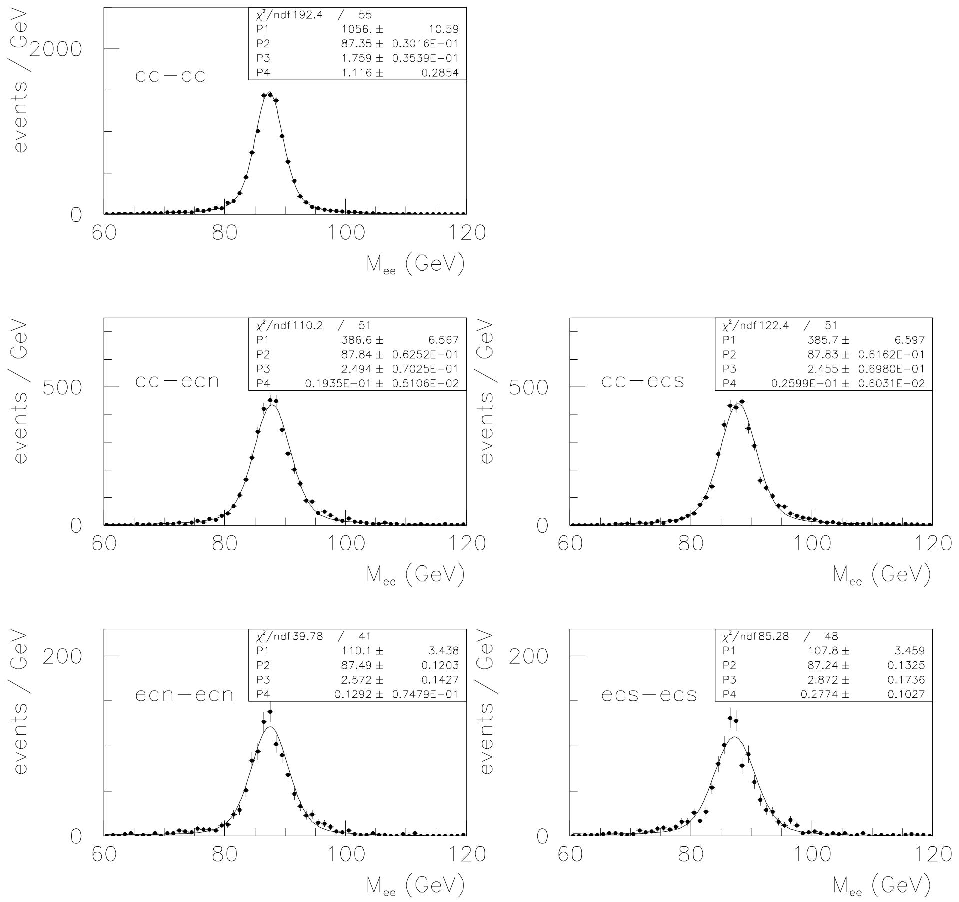

Figure 20: Fits to Monte Carlo to measure the Z width (P_3).

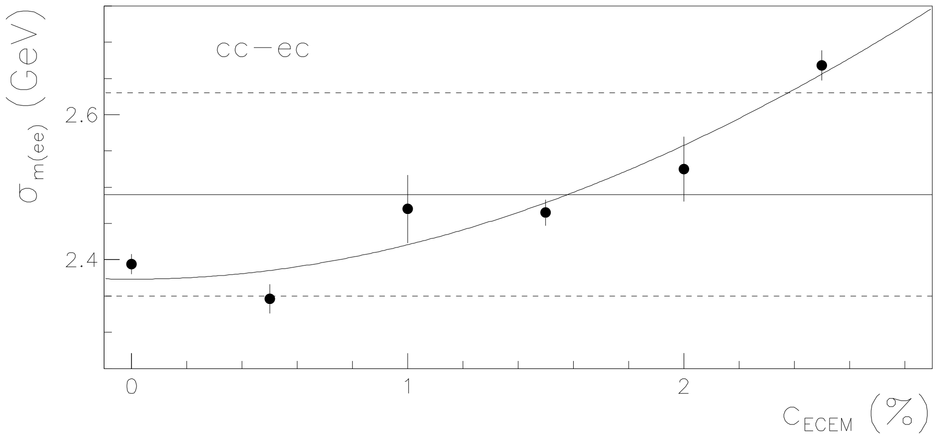

Figure 21: The dielectron mass resolution for CC-EC Z events as a function of the EC constant term. The horizontal lines show the data measurement and uncertainty.

9.2 Recoil Resolution

The width of the p_η balance and the p_ξ balance (where the ξ axis is perpendicular to the η axis) is sensitive to the recoil resolution. We compare the data and Monte Carlo for a recoil resolution of $0.49/\sqrt{u_T\ (\mathrm{GeV})}$ and $\alpha_{mb} = 1.032$ in figures 24-27. The p_η balance width is in good agreement between data and Monte Carlo for all Z topologies. Hence we use the same recoil resolution for EC W events as for the CC W events [1].

10 EM Response Offset

We parametrize the EM energy response as follows:

$$E_{measured} = \alpha\, E_{true} + \delta \tag{14}$$

where α is the EM energy scale and δ is the EM energy offset. At the high energies relevant for this analysis, the offset represents the effects of

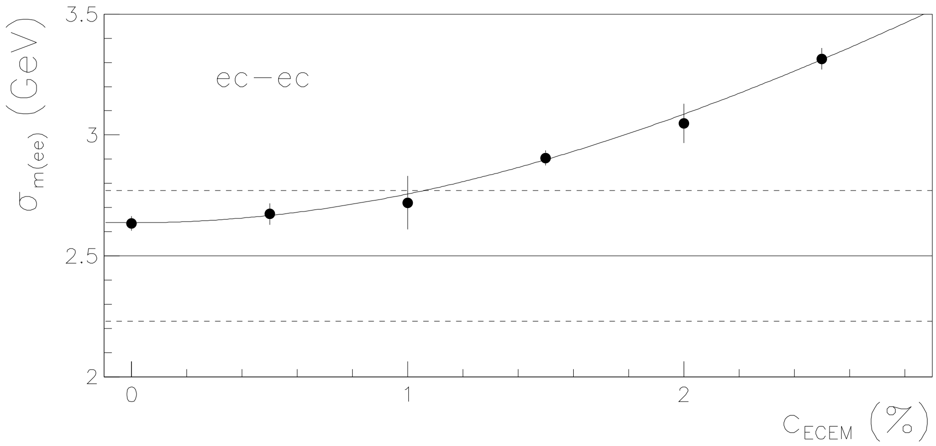

Figure 22: The dielectron mass resolution for EC-EC Z events as a function of the EC constant term. The horizontal lines show the data measurement and uncertainty.

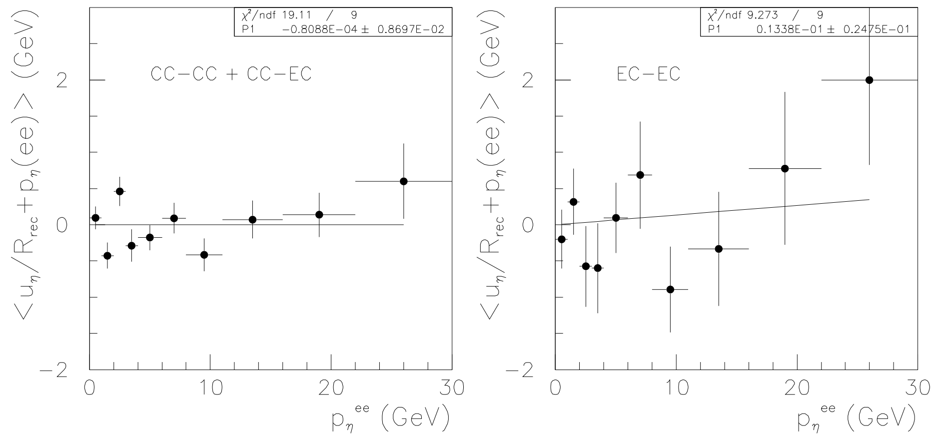

Figure 23: p_t balance measured using the $Z \to ee$ events of different topologies. The data are fitted for a proportionality.

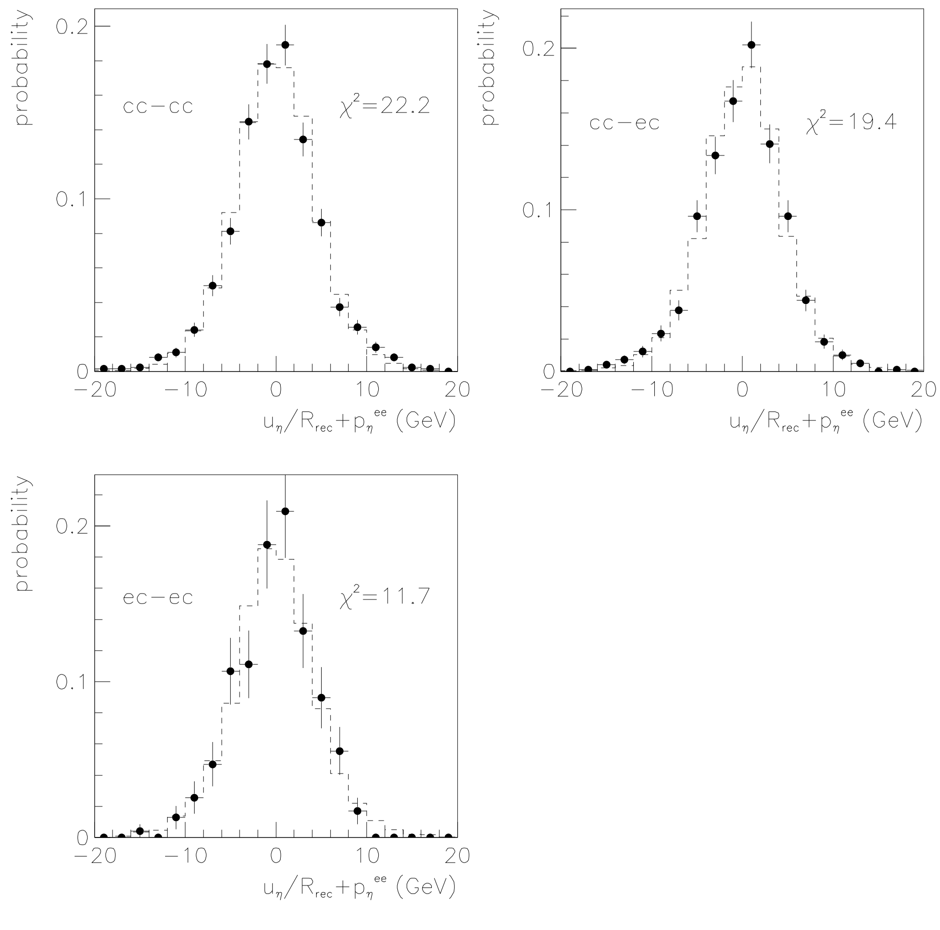

Figure 24: p_η balance measured using the $Z \to ee$ events of different topologies. The data (solid points) are compared to the Monte Carlo (dashed histogram).

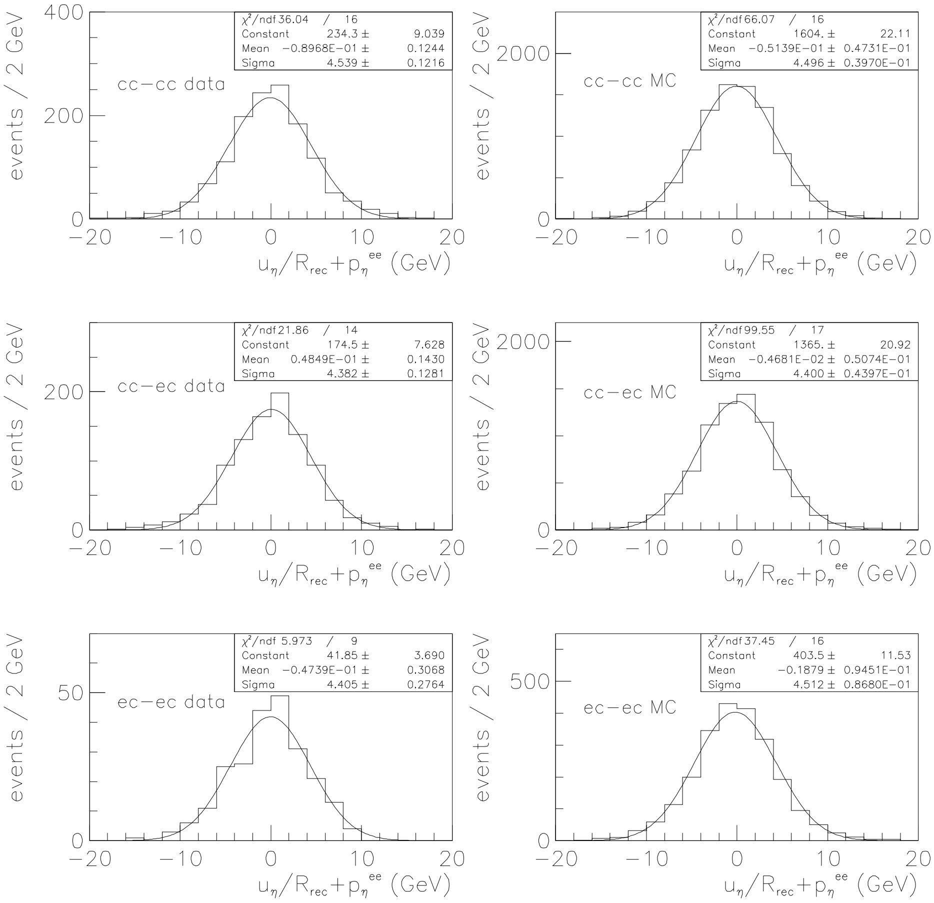

Figure 25: p_η balance measured using the $Z \to ee$ events of different topologies. The data (left) and the Monte Carlo (right) distributions are fit with Gaussians.

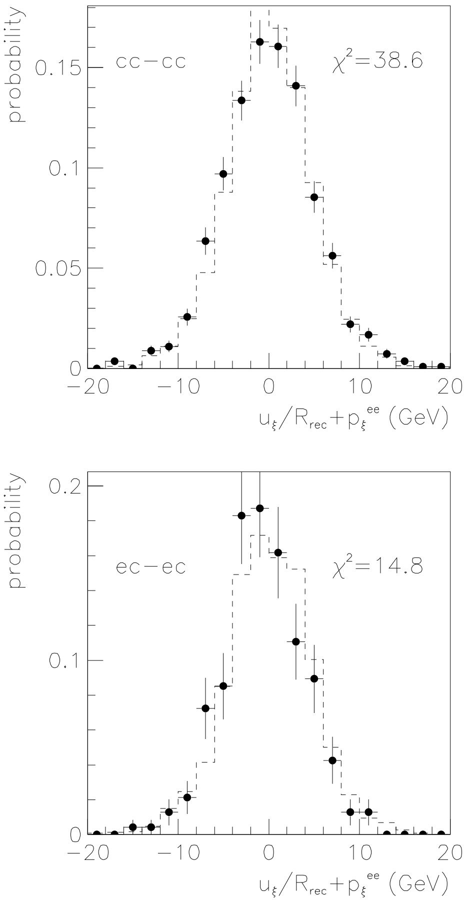

Figure 26: p_ξ balance measured using the $Z \to ee$ events of different topologies. The data (solid points) are compared to the Monte Carlo (dashed histogram).

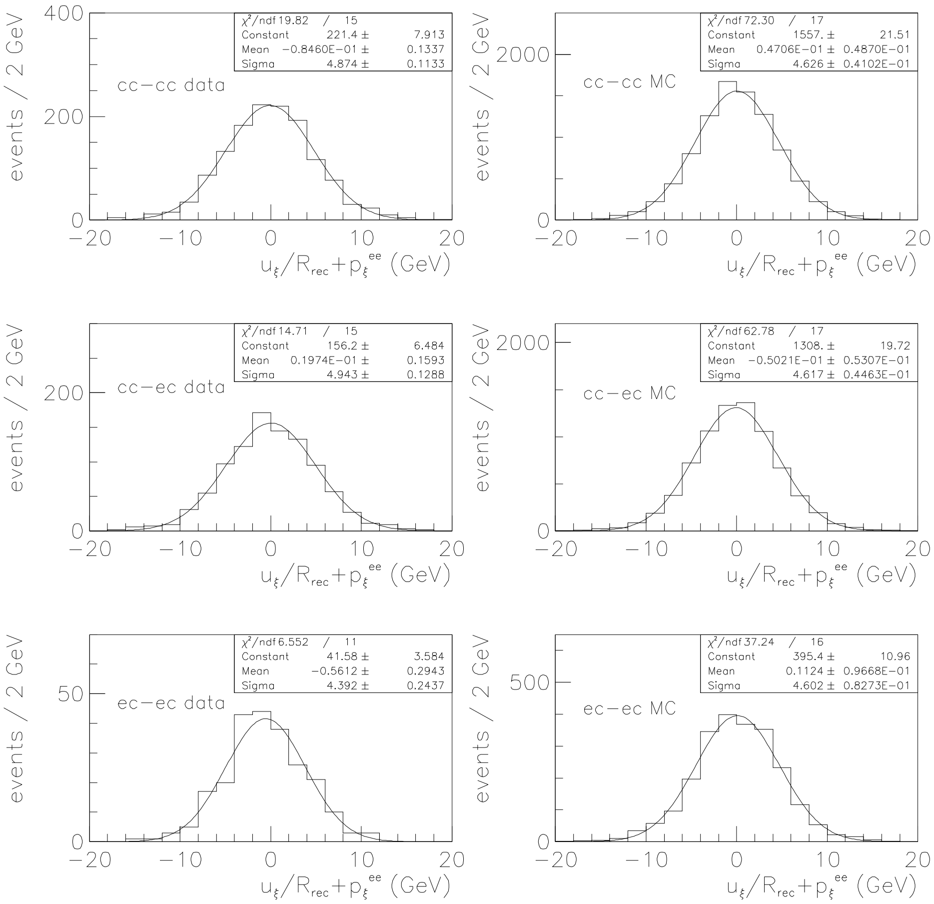

Figure 27: p_ξ balance measured using the $Z \to ee$ events of different topologies. The data (left) and the Monte Carlo (right) distributions are fit with Gaussians.

low energy non-linearities. We use the fact that the electrons in $Z \to ee$ events are not mono-energetic to constrain the EM offset in the EC, as was done for the CC [1]. The details of the offset measurement are given in [13]. The δ measurements obtained from the CC-ECN, CC-ECS, ECN-ECN and ECS-ECS $Z \to ee$ events are shown in figure 28. The offset measurements from the north and south calorimeters are consistent, as expected from the symmetric detector construction [14] of the calorimeters and the upstream material. The combined result for the EC EM offset is

$$\delta_{ec} = (-0.1 \ \pm \ 0.7) \text{ GeV} \tag{15}$$

11 $U_{||}$ Efficiency

We measure the EC electron identification efficiency as a function of $U_{||}$ using $Z \to ee$ events. We use the EM2_EIS_ESC trigger, and the EIS electron is used to tag the event. The ESC electron is then used to measure the efficiency. Background subtraction is performed using the sidebands. The details of this measurement are given in [15]. The $U_{||}$ efficiency measured in the EC is shown in figure 29. As a cross-check of our method, we use it to measure the $U_{||}$ efficiency in the CC. As shown in [15], we find consistency with the published result from [1].

12 Radiative Corrections

Due to the use of the fixed radius cone in the EC instead of the fixed $\eta\phi$ window, the algorithm for coalescing a radiated photon with the electron is modified in the Monte Carlo. Instead of coalescing when $R_{e\gamma} < 0.3$ (as in the CC), in the EC we coalesce when the distance $r_{e\gamma} < 20$ cm.

The change in the fitted W and Z masses due to two-photon radiation has been investigated [1], and the shifts vary between 5 and 10 MeV depending on the Z topology and the W fitted kinematic.

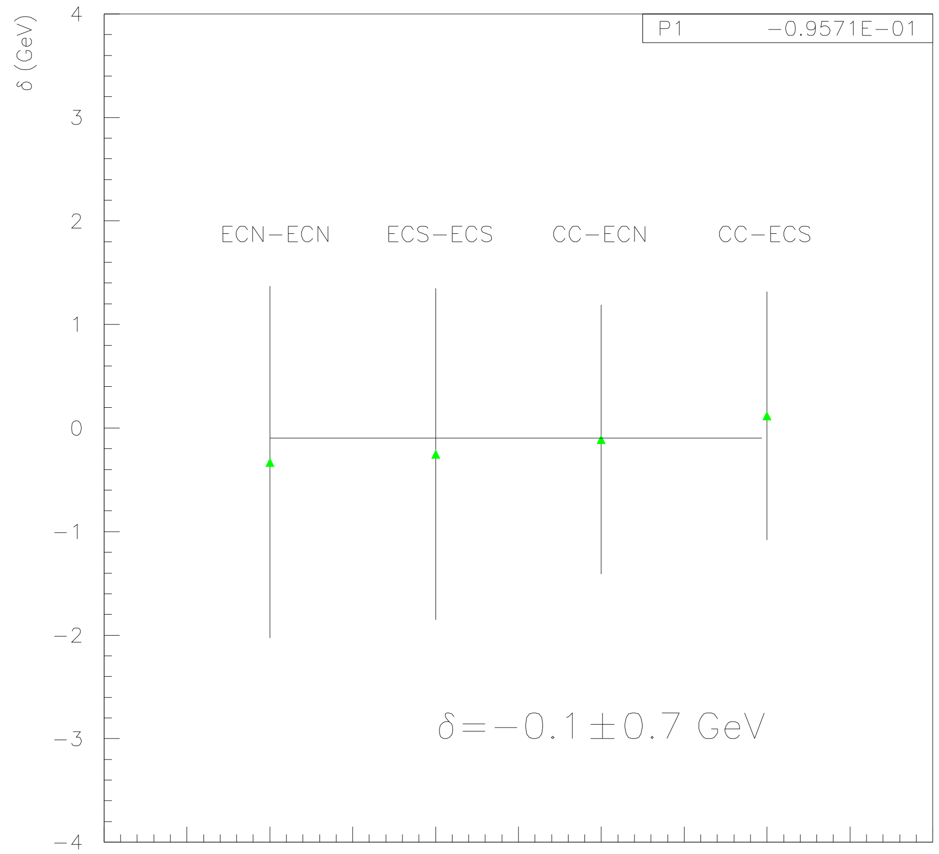

Figure 28: δ_{ec} measurements obtained from CC-ECN, CC-ECS, ECN-ECN and ECS-ECS $Z \rightarrow ee$ events respectively, and the combined measurement.

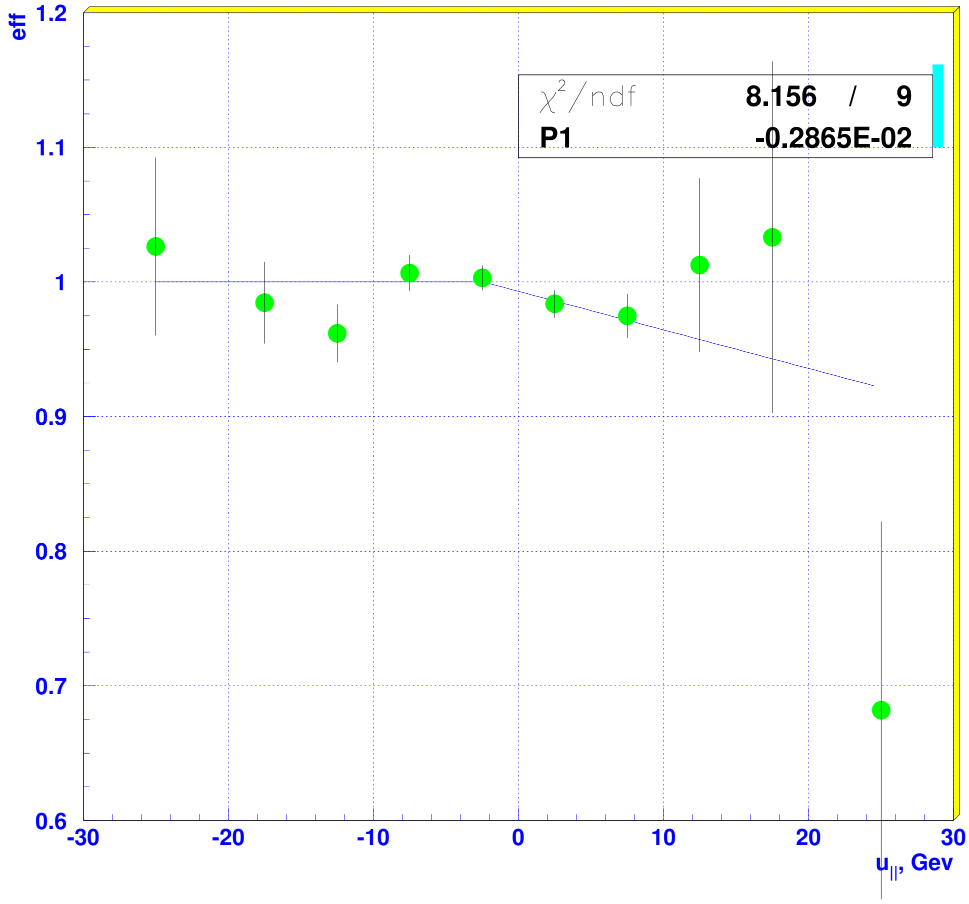

Figure 29: $U_{||}$ efficiency measurement in the EC, using $Z \to ee$ events.

13 Comparisons for W and Z Events

We compare distributions for the W recoil between data and Monte Carlo in figures 30 and 31. We also compare the distributions of the z position of the electron vertex in figure 32, and the (physics) η distributions of the electron in figure 33. The data and Monte Carlo are in good agreement. Figures 34 and 35 shows the comparison of the rapidity and p_t distributions of the Z between data and Monte Carlo. Figures 36 and 37 show the comparison between the electron energy distributions. Figure 38 shows the comparison between the instantaneous luminosity distributions for W and Z events. All the distributions compared are in good agreement.

14 Constraint on the W Production Model using the Electron η Distribution

In principle, if the acceptance for the $W \to e\nu$ decays were complete, the transverse mass distribution or the lepton p_t distributions would be independent of the W rapidity. However, cuts on the electron angle in the laboratory frame causes the observed distributions of the transverse momenta to depend on the W rapidity. Hence a constraint on the W rapidity distribution is useful in constraining the production model uncertainty on the W mass.

The pseudorapidity distribution of the electron from $W \to e\nu$ decays is correlated with the rapidity distribution of the W. Hence we compare the electron η distribution between data and Monte Carlo.

In order to compare the data with the Monte Carlo, we need to correct for the fake background in the data, and the electron identification efficiency, as a function of η. We obtain the fake background fraction as a function of η by counting the number of W events obtained with anti-electron cuts (see section 7) in bins of η, subtracting the 1.15% contamination due to good electrons, and normalizing the entire distribution to the total background fraction (separately in the CC and EC). The normalized background η distribution is subtracted from the η distribution of the data.

The electron identification efficiency (after fiducial and kinematic cuts) is measured using the CC-CC and CC-EC $Z \to ee$ events. All the electron identification cuts are used to identify one electron to tag the event. Candidates are selected in the mass range $81 < m_{ee} < 101$ GeV. Sidebands in

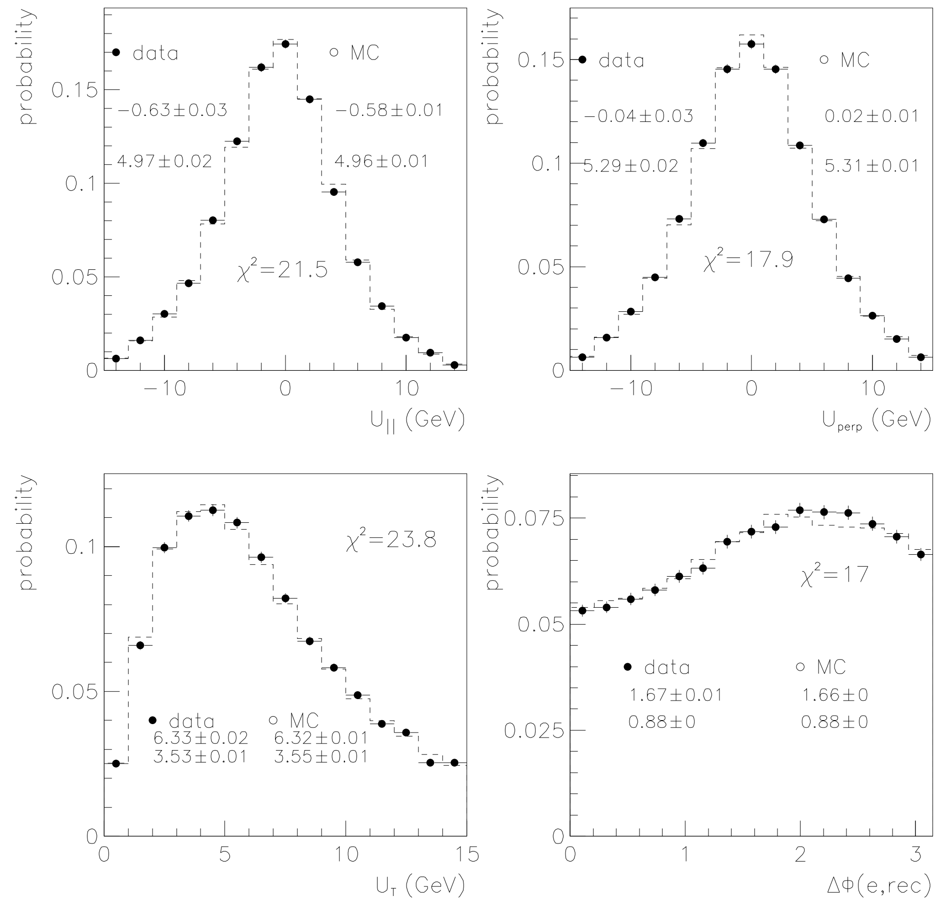

Figure 30: Comparisons of recoil distributions from CC W events between data (solid points) and Monte Carlo (dashed histogram). The upper number is the mean and the lower is the rms.

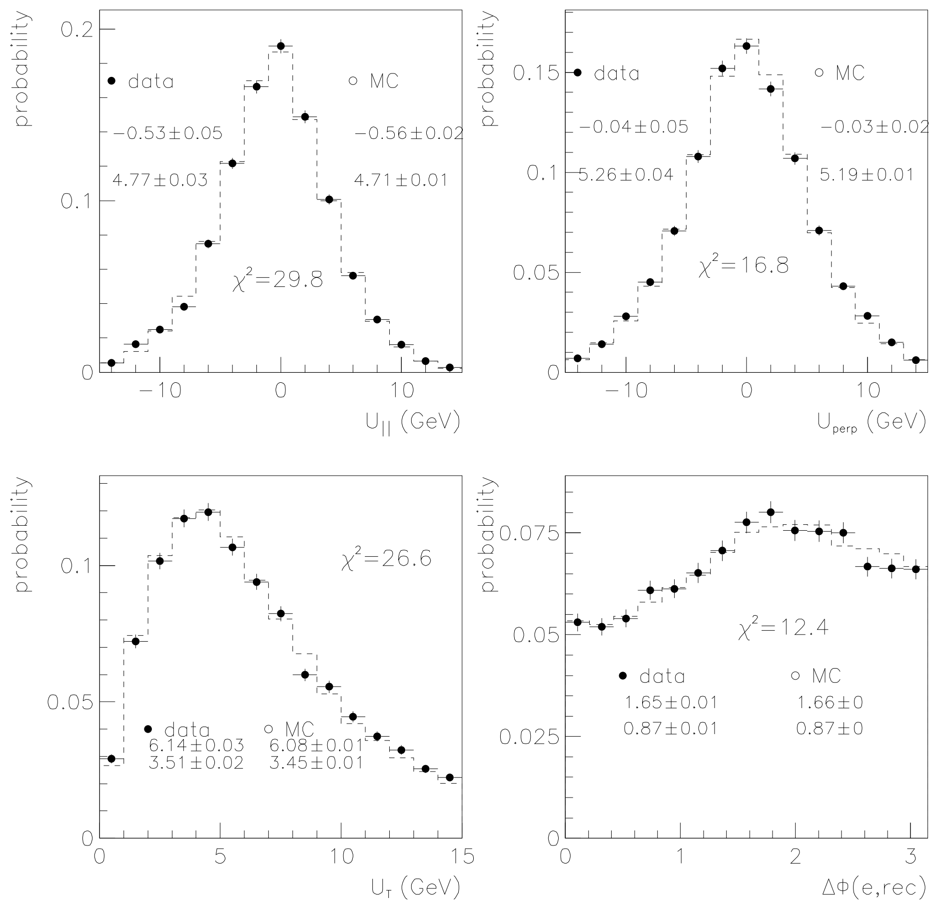

Figure 31: Comparisons of recoil distributions from EC W events between data (solid points) and Monte Carlo (dashed histogram). The upper number is the mean and the lower is the rms.

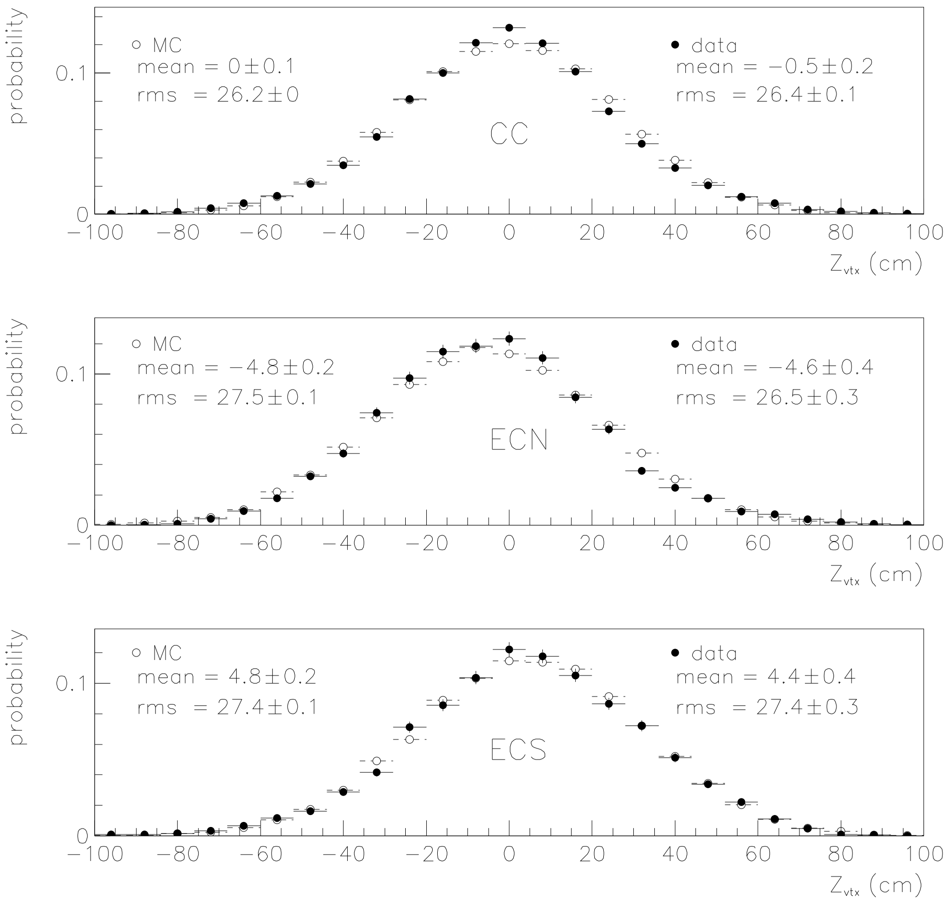

Figure 32: Comparisons of the z position of the electron vertex for $W \to e\nu$ data and Monte Carlo.

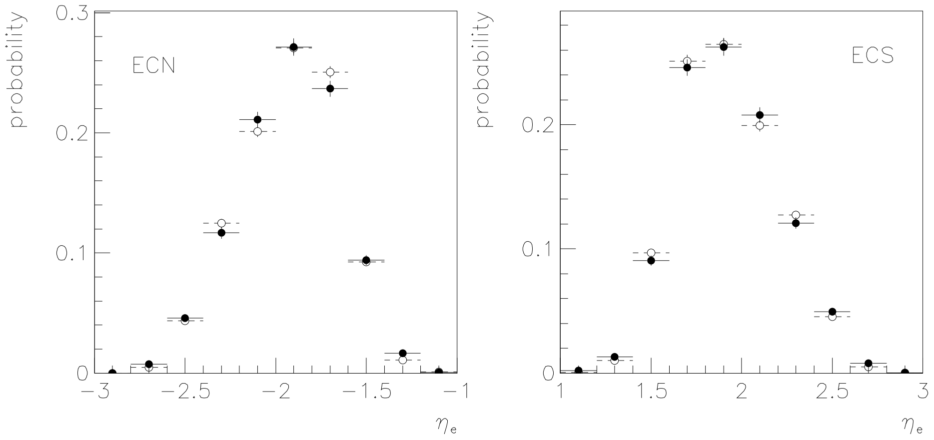

Figure 33: Comparisons of the (physics) η distributions of the electron for $W \to e\nu$ data (solid) and Monte Carlo (open).

the mass range $60 < m_{ee} < 70$ GeV and $110 < m_{ee} < 120$ GeV are used for background subtraction. The number of events in which the second electron also satisfies all the electron identification cuts is used to calculate the efficiency. The efficiency measured in bins of the second (probe) electron η is shown in figure 39.

We scale the electron η distribution predicted by the Monte Carlo, by the η-dependent efficiency, and compare to the background-subtracted data (see figure 40). The errors on the Monte Carlo points include the statistical errors on the Monte Carlo sample and the statistical errors on the efficiency measurements. The errors on the data points include the statistical errors on the number of candidate events and the statistical errors on the background estimate which has been subtracted. Figure 40 also shows the ratio between the background-subtracted data and the efficiency-corrected Monte Carlo, with the uncertainties mentioned above added in quadrature. The Monte Carlo has been normalized to the data. The χ^2 shown is with respect to unity.

In order to extract a constraint on the η distribution of the W, we intro-

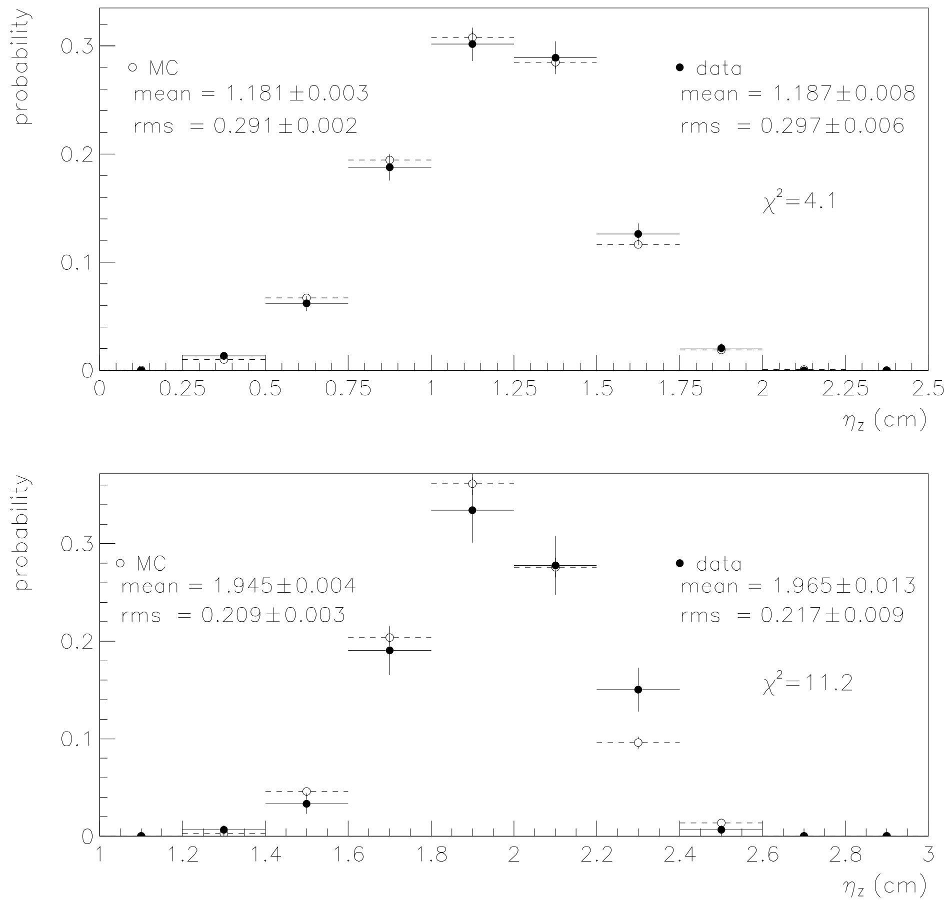

Figure 34: Comparisons of the rapidity ($|\ \eta\ |$) distributions of the Z for $Z \rightarrow ee$ data (solid) and Monte Carlo (open). The top plot is for CC-EC events and the bottom is for EC-EC events.

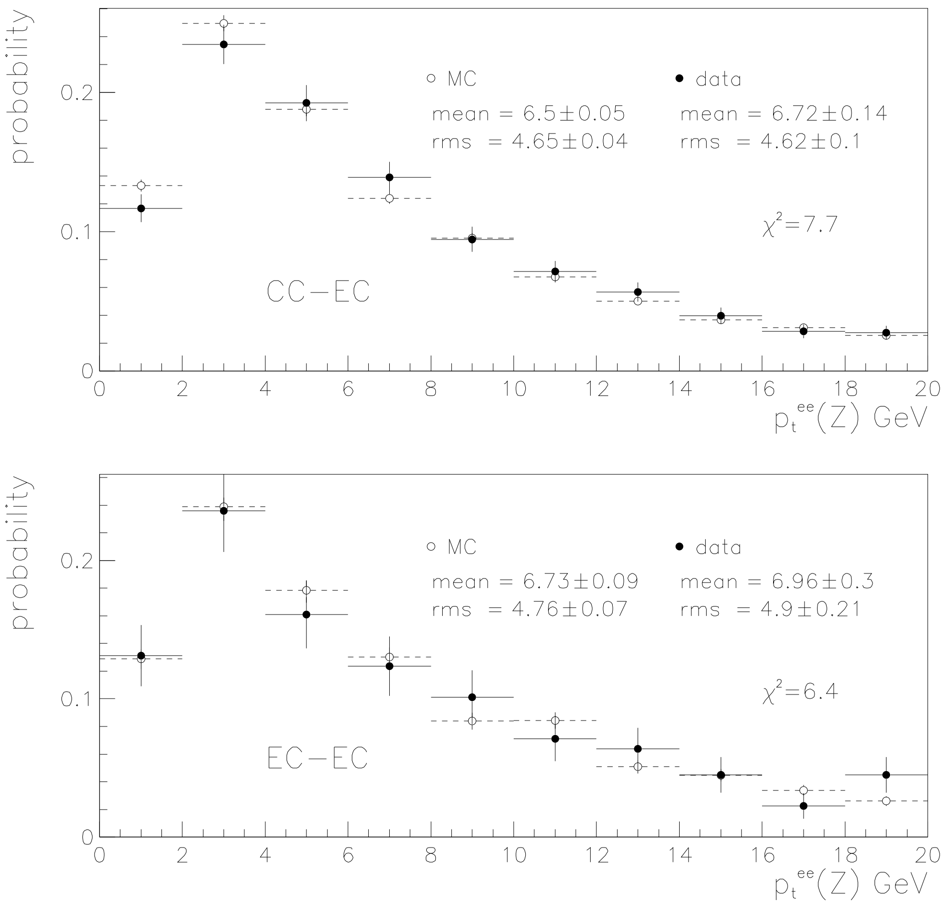

Figure 35: Comparisons of the p_t distributions of the Z for $Z \rightarrow ee$ data (solid) and Monte Carlo (open).

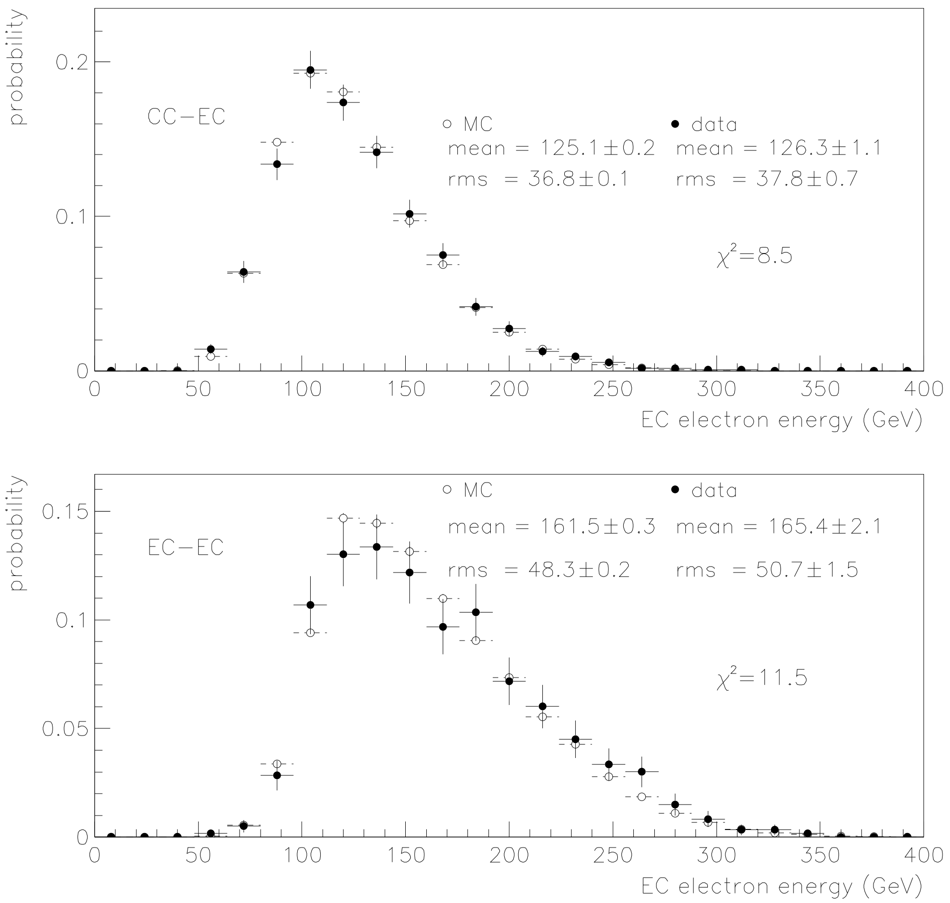

Figure 36: Comparisons of the EC electron energy distributions for $Z \to ee$ data (solid) and Monte Carlo (open).

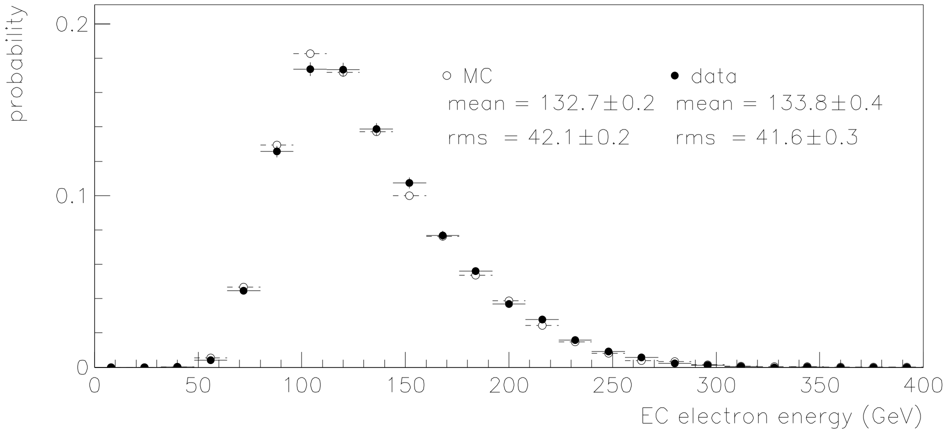

Figure 37: Comparisons of the EC electron energy distributions for $W \rightarrow e\nu$ data (solid) and Monte Carlo (open).

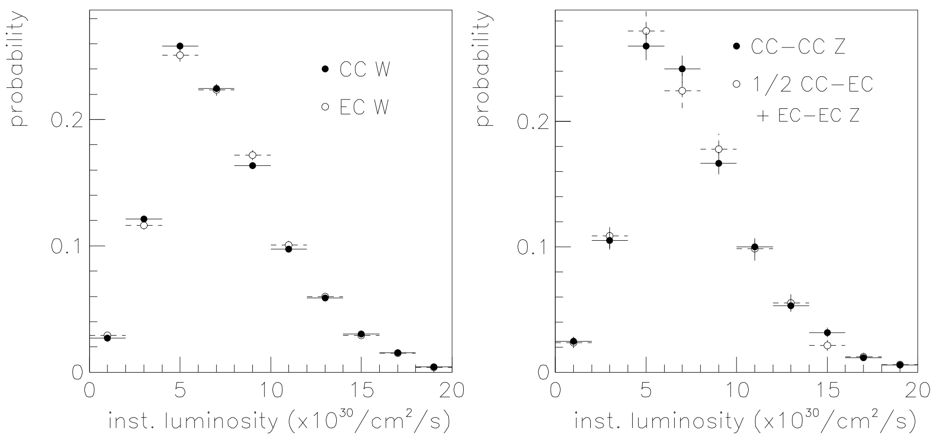

Figure 38: Comparisons of the luminosity distributions for CC and EC W and Z events.

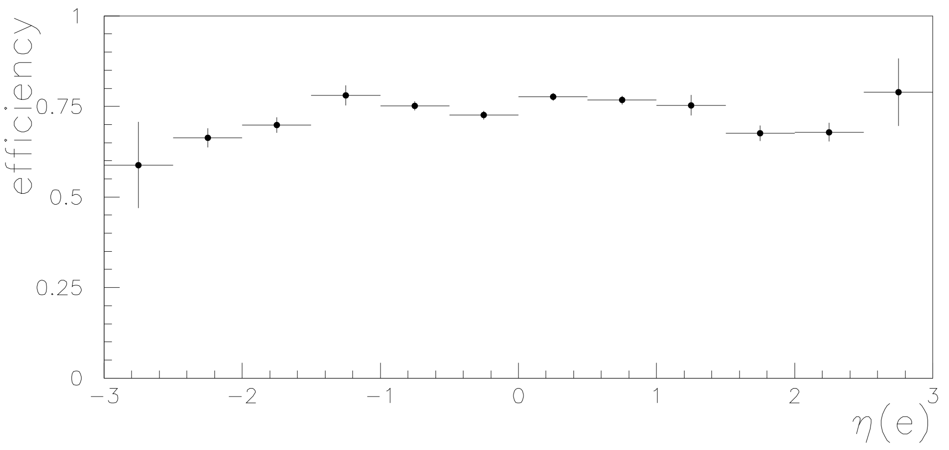

Figure 39: Dependence of electron identification efficiency on electron pseudorapidity. Statistical errors are shown.

duce in the CMS Monte Carlo a scale factor as follows:

$$\eta_W \to k_\eta \cdot \eta_W \tag{16}$$

i.e. the rapidity of the W is scaled with the factor k_η. We then compute the χ^2 between the data and Monte Carlo $\eta(e)$ distributions for different k_η. The result is shown in figure 41 for four different parton distribution functions. Table 2 shows the values of k_η at which the χ^2 is minimized for the different pdf's.

Table 2: χ^2 minimizing value of k_η for different pdf's.

MRSA′	CTEQ3M	CTEQ2M	MRSD-′
0.975	0.98	0.985	0.99

The uncertainty in k_η is 1.6%. We generate Monte Carlo events with different values of k_η and fit them with templates generated with k_η set to

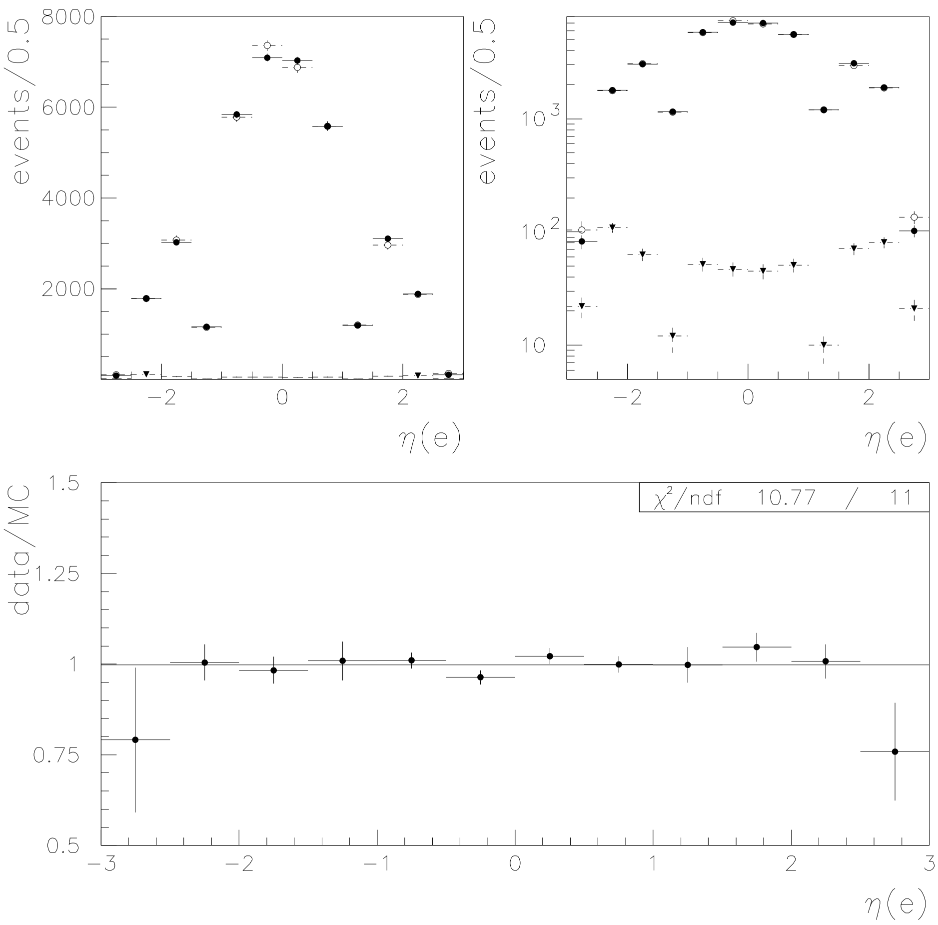

Figure 40: (top) η distribution of the electron from $W \to e\nu$ decays from background-subtracted data (solid circles), efficiency-corrected Monte Carlo (open circles) and the fake background (solid triangles). The distributions are shown on a linear (top left) and logarithmic (top right) scale. (bottom) The ratio of the background-subtracted data and efficiency-corrected Monte Carlo. The Monte Carlo has been normalized to the data. The χ^2 is with respect to unity.

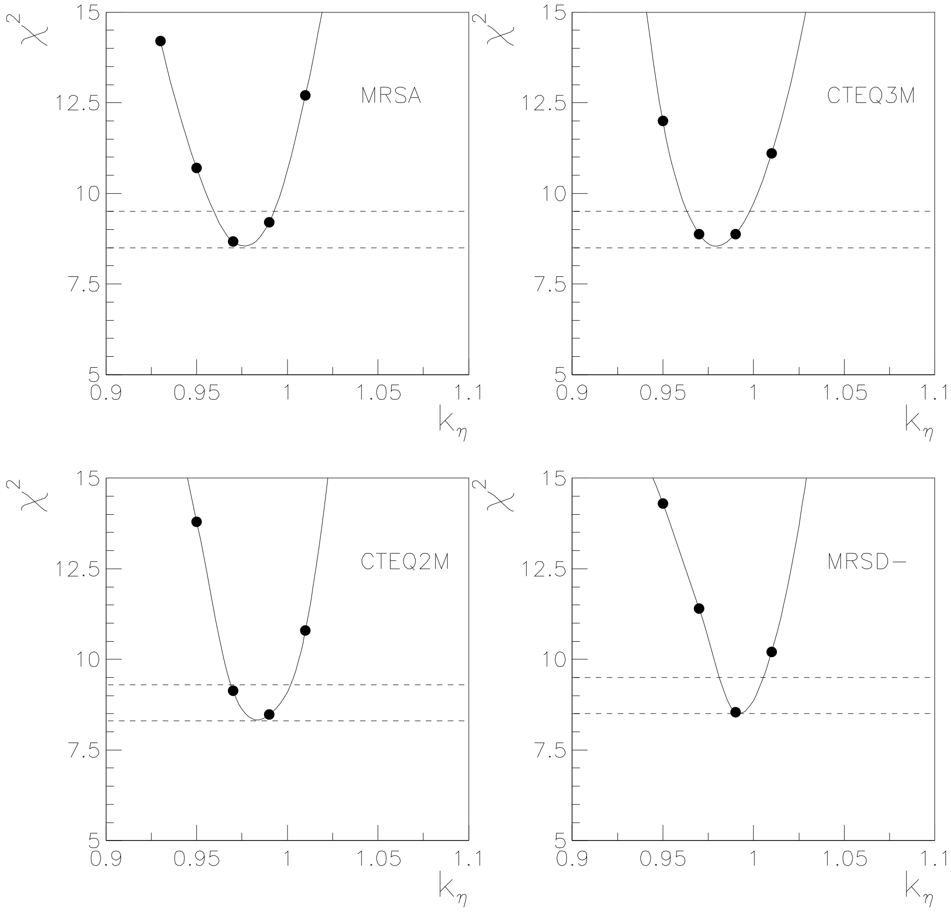

Figure 41: χ^2 of the electron η distribution ratio between data and Monte Carlo from unity, as a function of the W rapidity scale factor k_η. There are 11 degrees of freedom.

unity. For a true W pole mass of 80.4 GeV, figure 42 shows the fitted W mass as a function of k_η. For a k_η variation of 1.6%, the variation of the fitted W mass in the EC is shown in table 3.

Table 3: Variation in fitted EC W mass due to 1.6% variation in k_η.

	m_t fit	$p_t(e)$ fit	$p_t(\nu)$ fit
δM_W (MeV)	34	48	25

We investigate the possible correlation between the W p_t and rapidity spectra by studying the dependence of the mean $p_t(W)$ on k_η. As shown in figure 43 there is no correlation for CC W's, while $< p_t(W) >$ for EC W's is lower and increases towards the CC value with increasing k_η. This is because the forward W's are becoming more central. For a 1.6% variation of k_η, the change in $< p_t(W) >$ for EC W's is 8 MeV, which is negligible compared to the $\sim$100 MeV uncertainty on $< p_t(W) >$. Hence we can neglect any correlation between the W rapidity and p_t spectra for the k_η analysis.

15 Mass Fits

Figures 44-45 show the fits to the Z mass spectra in the range $70 < m_{ee} < 110$ GeV. Also shown are the ln(likelihood) maxima and the χ^2 of the maximum-likelihood fits. The fits [16] are performed in the range $60 < m_t < 90$ GeV, $30 < p_t^e < 50$ GeV and $30 < p_t^\nu < 50$ GeV for CC W events, and $65 < m_t < 90$ GeV, $33 < p_t^e < 50$ GeV and $33 < p_t^\nu < 50$ GeV for EC W events. Figures 46-48 show maximum likelihood fits to the m_t, p_t^e and p_t^ν distributions of the CC and EC W events. Also shown are the signed χ distributions for the fits and the ln(likelihood) maxima.

The results of the fits to the data from the north and south cryostats separately and the combined samples are as follows:

$$
\begin{aligned}
M_Z &= 91.187 \pm 0.075 \text{ GeV (CC} - \text{CC)} \\
M_Z &= 91.123 \pm 0.178 \text{ GeV (CC} - \text{ECN)} \\
M_Z &= 91.596 \pm 0.316 \text{ GeV (ECN} - \text{ECN)}
\end{aligned}
$$

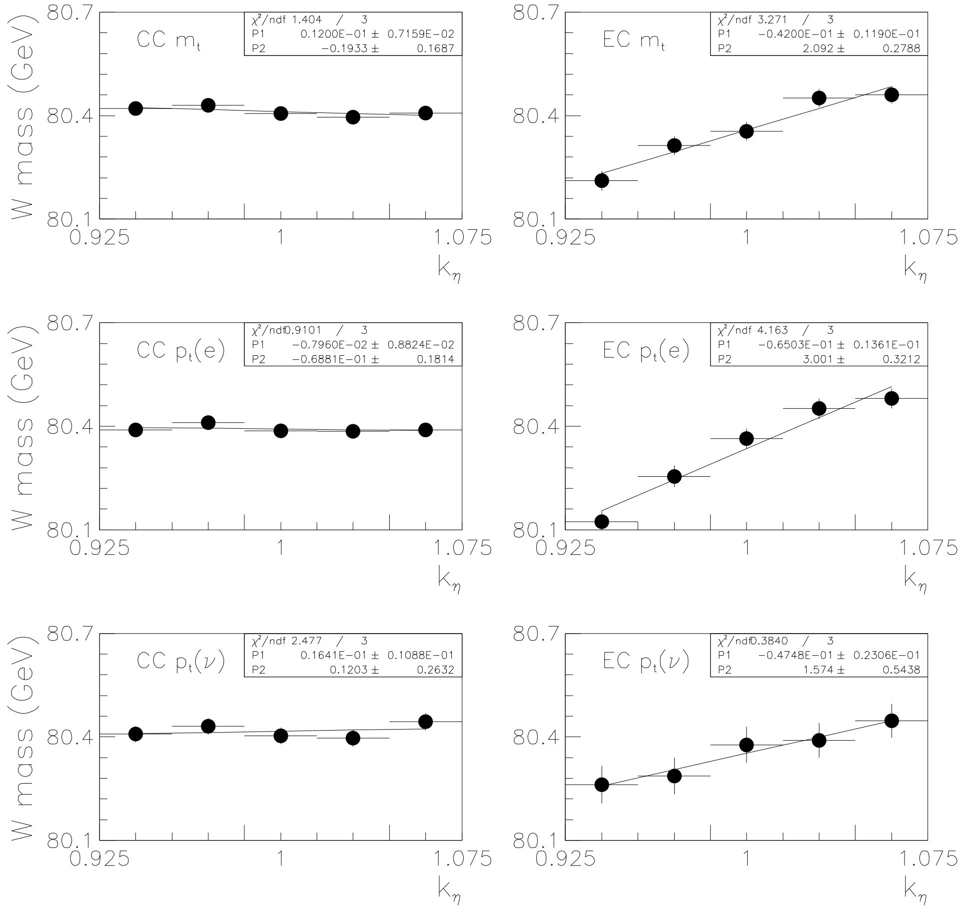

Figure 42: Fitted W mass for MC experiments generated with different k_η, and a true W mass of 80.4 GeV.

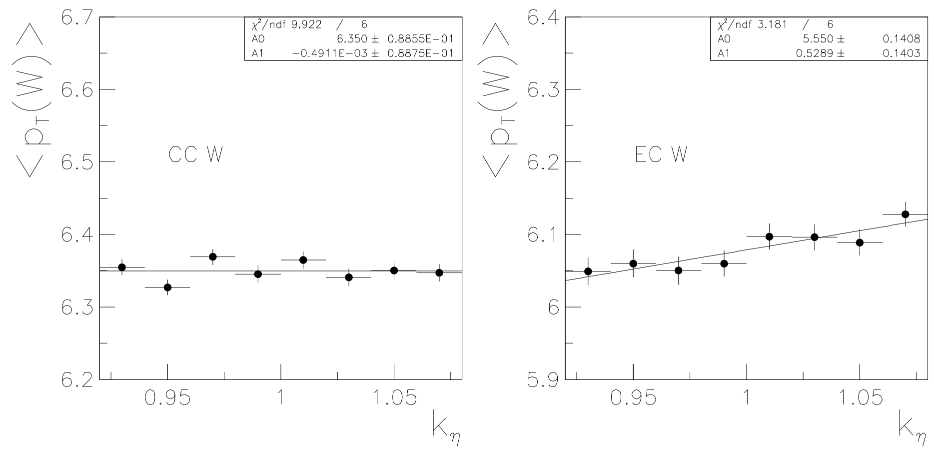

Figure 43: Monte Carlo prediction for the dependence of mean $p_t(W)$ on k_η. The straight line is a fit to the points.

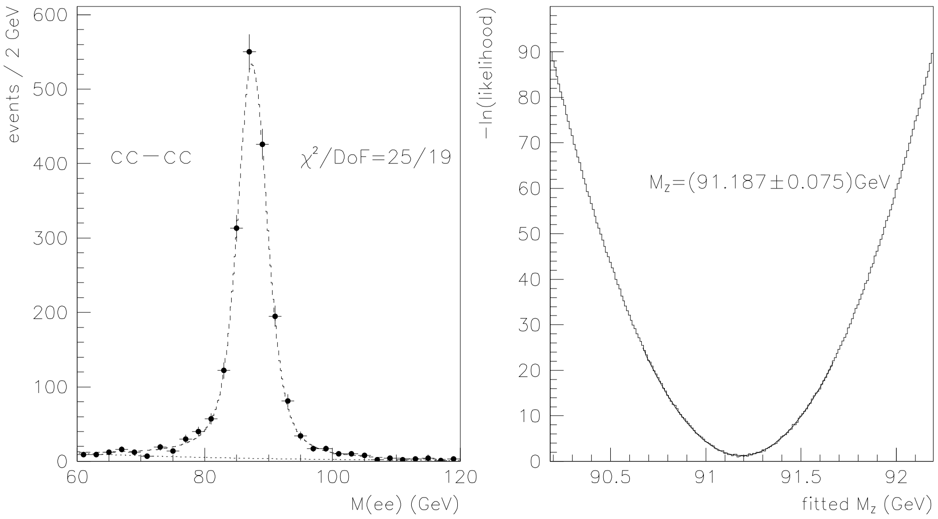

Figure 44: Maximum-likelihood fit to the CC-CC Z events.

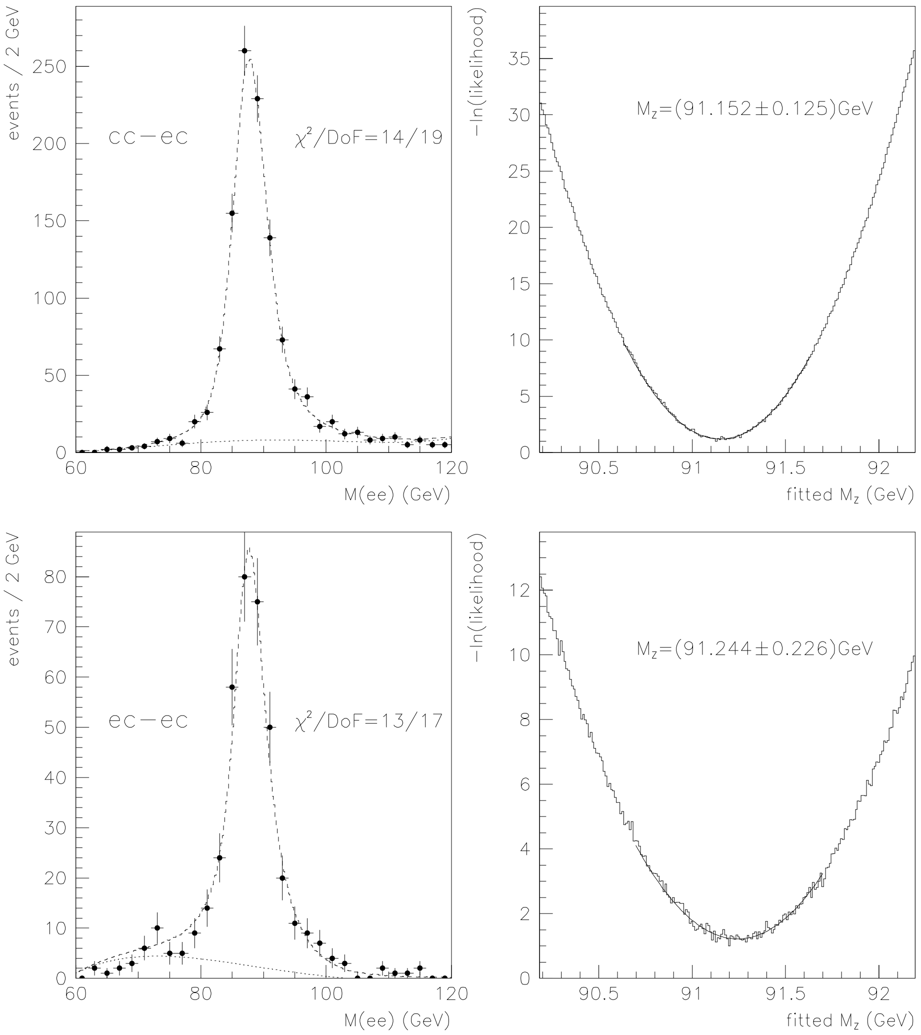

Figure 45: Maximum-likelihood fits to the CC-EC and EC-EC Z events.

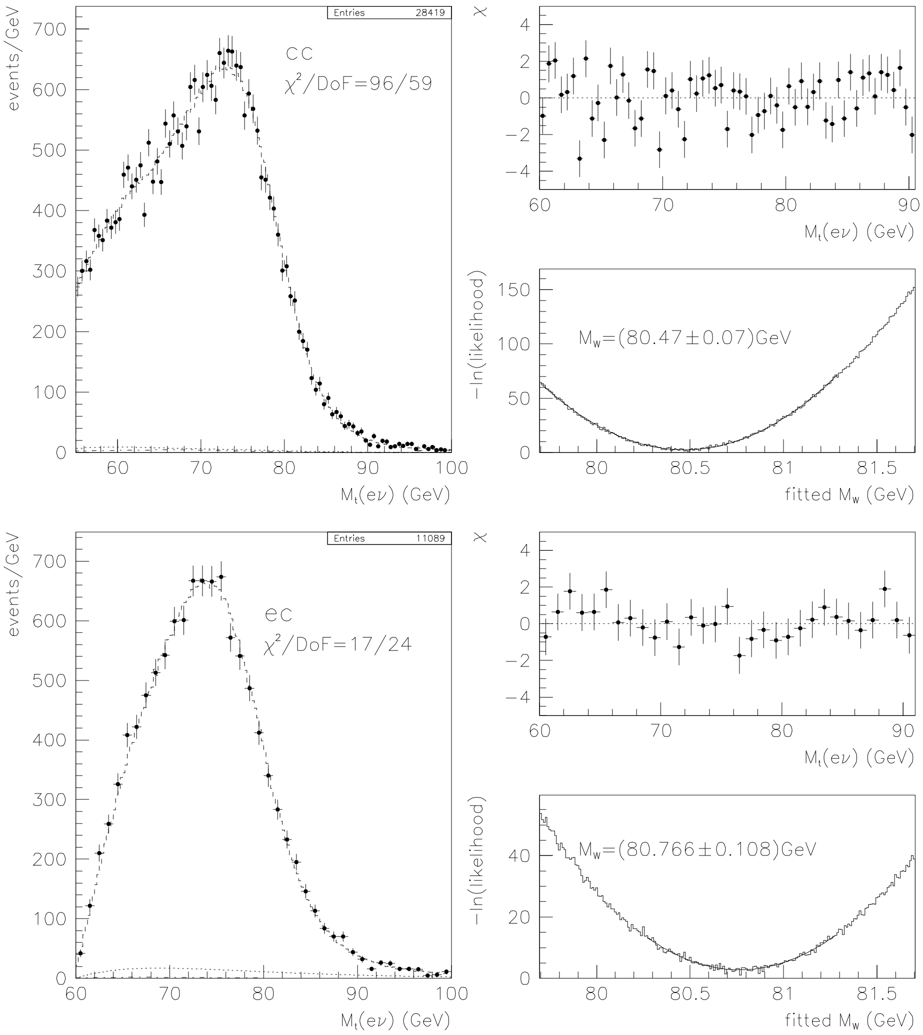

Figure 46: Maximum-likelihood fit to the m_t distributions of the W events.

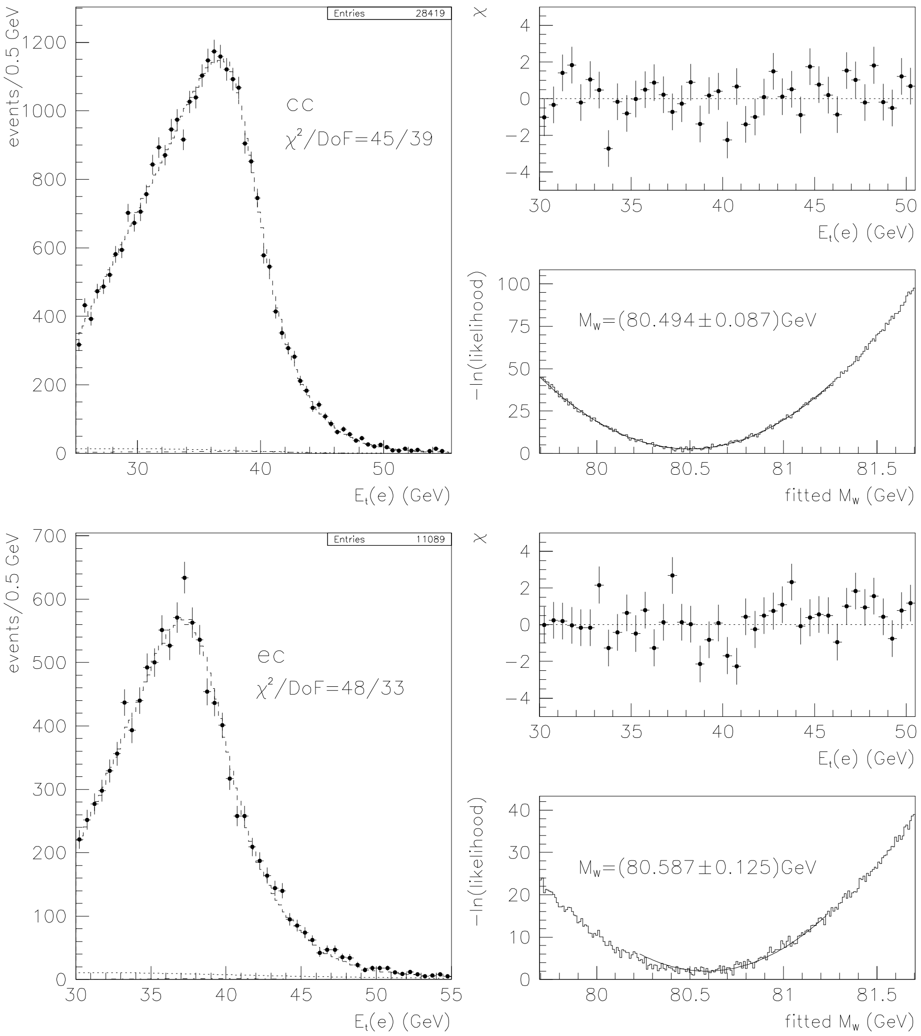

Figure 47: Maximum-likelihood fits to the electron p_t distributions of the W events.

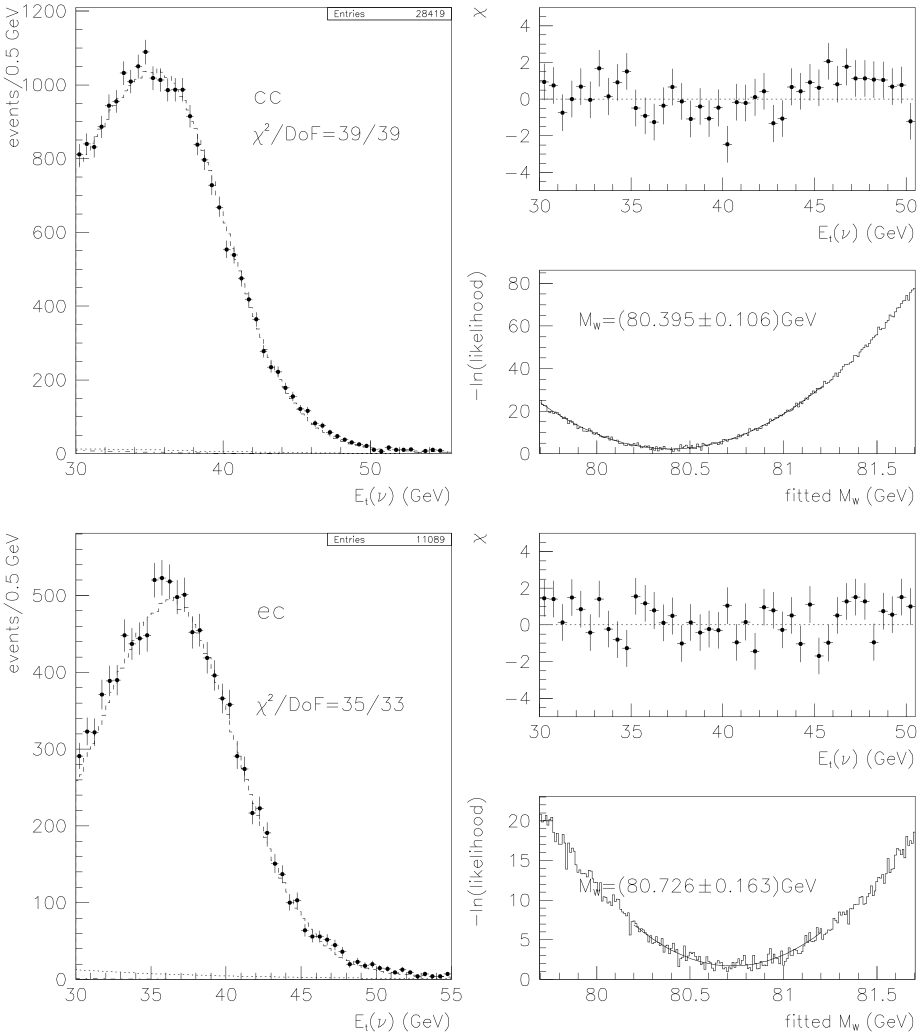

Figure 48: Maximum-likelihood fits to the p_t^ν distributions of the W events.

$$
\begin{aligned}
M_Z &= 91.178 \pm 0.174 \text{ GeV (CC – ECS)} \\
M_Z &= 90.918 \pm 0.303 \text{ GeV (ECS – ECS)} \\
M_Z &= 91.152 \pm 0.125 \text{ GeV (CC – EC)} \\
M_Z &= 91.244 \pm 0.226 \text{ GeV (EC – EC)}
\end{aligned} \tag{17}
$$

$$
\begin{aligned}
M_W &= 80.470 \pm 0.070 \text{ GeV (CC } m_t \text{ fit)} \\
M_W &= 80.494 \pm 0.087 \text{ GeV (CC } p_t^e \text{ fit)} \\
M_W &= 80.395 \pm 0.106 \text{ GeV (CC } p_t^\nu \text{ fit)} \\
\\
M_W &= 80.796 \pm 0.150 \text{ GeV (ECN } m_t \text{ fit)} \\
M_W &= 80.430 \pm 0.172 \text{ GeV (ECN } p_t^e \text{ fit)} \\
M_W &= 80.744 \pm 0.241 \text{ GeV (ECN } p_t^\nu \text{ fit)} \\
\\
M_W &= 80.763 \pm 0.147 \text{ GeV (ECS } m_t \text{ fit)} \\
M_W &= 80.643 \pm 0.186 \text{ GeV (ECS } p_t^e \text{ fit)} \\
M_W &= 80.729 \pm 0.210 \text{ GeV (ECS } p_t^\nu \text{ fit)} \\
\\
M_W &= 80.766 \pm 0.108 \text{ GeV (EC } m_t \text{ fit)} \\
M_W &= 80.587 \pm 0.125 \text{ GeV (EC } p_t^e \text{ fit)} \\
M_W &= 80.726 \pm 0.163 \text{ GeV (EC } p_t^\nu \text{ fit)}
\end{aligned} \tag{18}
$$

The published results from [1] are

$$
\begin{aligned}
M_W &= 80.438 \pm 0.070 \text{ GeV (CC } m_t \text{ fit)} \\
M_W &= 80.475 \pm 0.087 \text{ GeV (CC } p_t^e \text{ fit)} \\
M_W &= 80.370 \pm 0.110 \text{ GeV (CC } p_t^\nu \text{ fit)}
\end{aligned} \tag{19}
$$

As a cross-check, we fit the transverse mass distribution of the $Z \to ee$ events, reconstructed using each electron and the recoil. The fitting range is $70 < m_t < 100$ GeV for the CC-CC and EC-EC events and $70 < m_t < 90$ GeV for the CC-EC events. Figures 49 and 50 show the results. The fits are good and the fitted masses are consistent with the known Z mass. There is a small excess in the data above the MC in the low transverse mass tail for the CC-CC Z events. This might be due to the angular distribution of the Z decay not being modelled in the MC as completely as the W is modelled. For instance, the sea-sea fraction of quarks involved in Z production would affect the Z polarization and hence the decay as it does for the W, but we do not model this. The reason is that we use the Z invariant mass to set the EM scale, which is not sensitive to the angular distribution. Since the Z mass extracted from the transverse mass fit is mostly sensitive to the Jacobian edge, the low tail does not influence the fitted mass.

The EC transverse mass fits provide a consistency check with an uncertainty of 284 MeV.

As another cross-check, the published data[2] from [1] was fit with the Monte Carlo templates used in this analysis. The results agreed with the values presented here within 15 MeV. Similarly, the MC templates used in this analysis were used to fit a high-statistics CC Monte Carlo experiment from the published analysis. The fitted value agreed with the generated value within 7 MeV (9 MeV, 11 MeV) for the m_t ($p_t(e)$, $p_t(\nu)$) fit. This shows that the data and the Monte Carlo used in the two CC analyses are consistent.

16 Systematic Variations

We vary the various detector parameters and calibrations to quantify the resulting variation on the extracted W and Z mass.

The uncertainties on the electron angular scale arise from the statistical and systematic uncertainties on the FDC radial calibration, and the statistical error (from $Z \to ee$ events) on the relative radial calibration of the FDC and the EC. The systematic uncertainty on the FDC radial calibration scale amounts to 0.3×10^{-3} from the vertex calibration, 0.14×10^{-3} due to the FDC alignment and 0.17×10^{-3} due to Muon chamber alignment uncertainties [17], for a total of 0.37×10^{-3}. The statistical uncertainty on the FDC radial calibration is 0.39×10^{-3} (figure 5), for a total uncertainty of 0.54×10^{-3}. The radial cross-calibration of the EC with the FDC gives a statistical error on the EC scale of 0.31×10^{-3} (figure 6).

In the data, we change the FDC and EC scale together by 0.54×10^{-3}, and the EC scale alone by 0.31×10^{-3}, giving the variations in the fitted W and Z masses shown in table 4. We also change the EC electron energy by

[2]kindly provided by Eric Flattum.

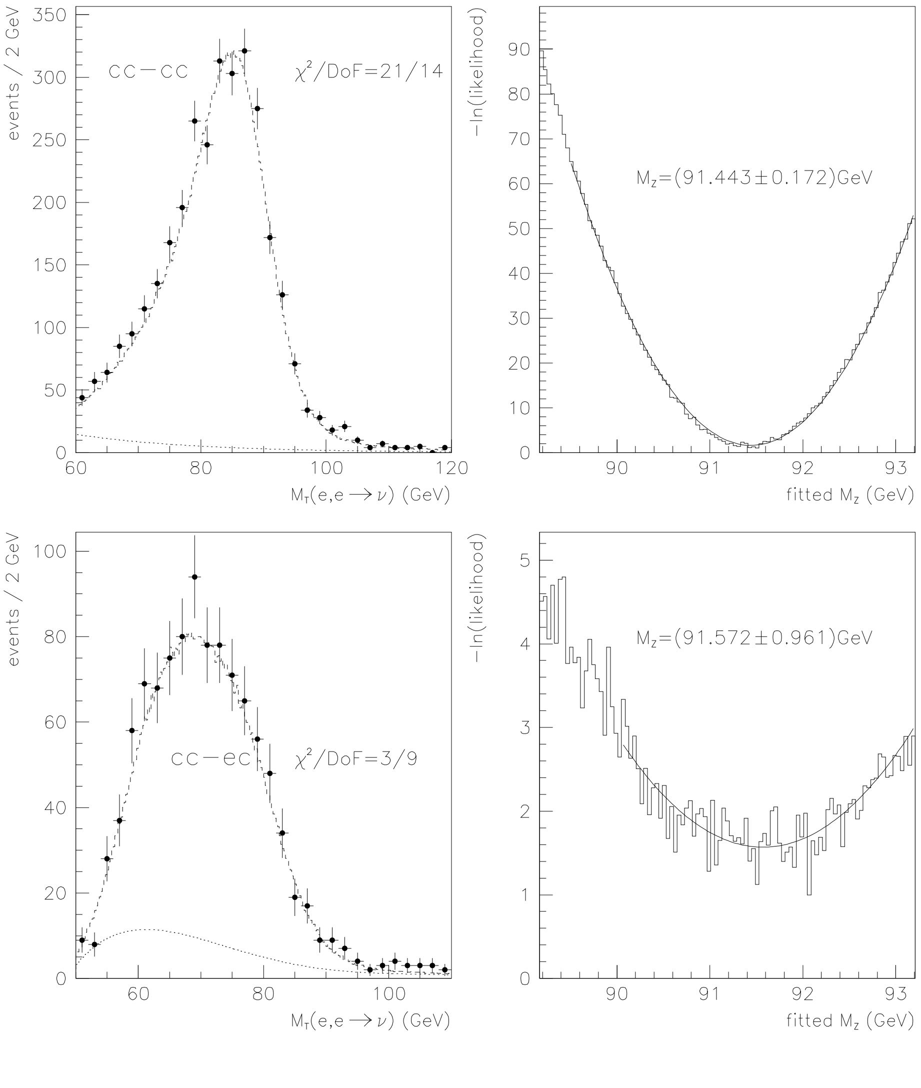

Figure 49: Maximum-likelihood fits to the transverse mass distributions of the CC-CC and CC-EC Z events, where the transverse mass is reconstructed using the central electron(s) and the recoil.

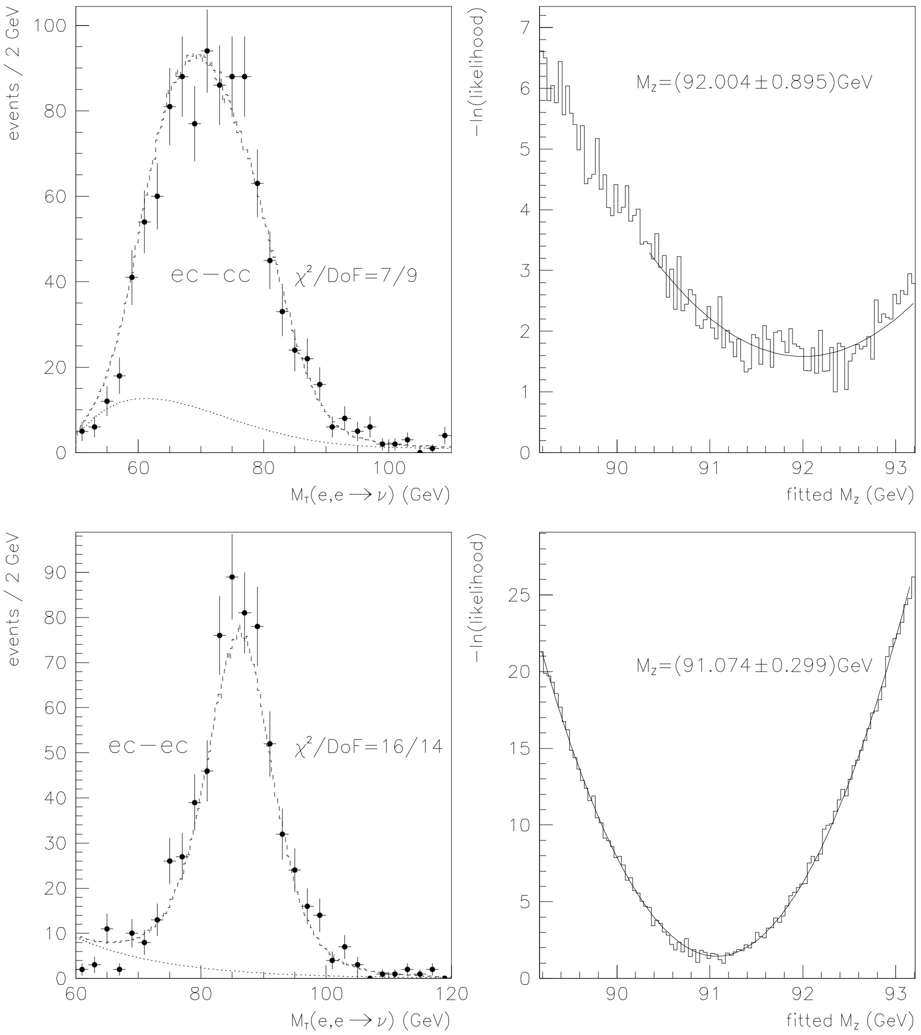

Figure 50: Maximum-likelihood fits to the transverse mass distributions of the EC-CC and EC-EC Z events, where the transverse mass is reconstructed using the forward electron(s) and the recoil.

0.7 GeV due to the uncertainty on the EM energy offset [13], to observe the change on the fitted W and Z masses. We also change the QCD background normalization and shape by one standard deviation.

We calculate analytically the effect of varying the CC EM energy scale and the EC EM energy scale.

Other systematics are evaluated by generating Monte Carlo events with changed parameters, and fitting with the standard Monte Carlo templates. The parton luminosity slope parameter β is varied by 0.001. The EC constant term is varied according to equation 12. We vary the p_t-independent hadronic response term α_{rec} (equation 13) by 0.012. We change the pair of correlated hadronic resolution parameters (s_{rec}, α_{mb}) by $(\pm 0.14, \mp 0.028)$ and $(\pm 0.08, \pm 0.012)$ to obtain orthogonal variations, which we combine in quadrature. We also change α_{mb} independently by 0.01 which is the uncertainty in the difference between the hadronic resolution in Z and W events. These uncertainties in the hadronic resolution parameters are taken from [1]. We vary $\Delta U_{||}/d\eta d\phi$ by 14 MeV and the coalescing radius for radiative events by 7 cm, which represents the same fractional change on the 20 cm cone as was performed in [1] for the CC analysis.

The MRSA parton distribution functions are used in the extraction of the W mass from the data. The same MC spectra are used to fit the Monte Carlo experiments generated using the MRSA, MRSD-', CTEQ3M and CTEQ2M pdf's respectively. The variation of the fitted values from the MRSA experiment are quoted in table 4.

17 Extracting the W Mass

17.1 Electromagnetic Scale

We first extract the EM scale for the EC, relative to electromagnetic scale used in the Monte Carlo simulation. From the Z mass fits and statistical errors given in equation 17, and the LEP Z mass of 91.187 GeV, we obtain the following:

$$\begin{aligned} \alpha_{ec} &= 0.99924 \pm 0.00274 \ \ (\mathrm{CC-EC}) \\ \alpha_{ec} &= 1.00063 \pm 0.00248 \ \ (\mathrm{EC-EC}) \end{aligned} \tag{20}$$

Table 4: Variation in extracted M_W and M_Z (in MeV) from forward electron sample due to various sources.

Source	δM_Z (CC-EC)	δM_Z (EC-EC)	δM_W (m_t)	δM_W (p_t^e)	δM_W (p_t^ν)
FDC radial scale	8	36	43	37	28
FDC-EC radial scale	10	52	57	54	48
0.7 GeV EM offset	284	421	437	433	386
EC EM scale variation 0.004	182	365	322	322	322
CC EM scale variation 0.0008	37	0	0	0	0
QCD background normalization	0	11	-12	-15	-25
QCD background shape		-5	-16	-23	-78
parton luminosity β	-8	-7	-9	-11	-18
EM constant term c_{ecem}			45	29	78
α_{rec} hadronic response			-11	-20	50
Z hadronic resolution			37	3	189
$Z \to W$ hadronic resolution			15	-2	73
$U_{\|\|}$ correction	10	15	9	17	-3
$U_{\|\|}$ efficiency			4	-22	40
$r_0^{e\gamma}$	10	13	9	17	12
2γ	5	10	5	10	0
$P_T(W)$ spectrum			22	37	44
MRSD-' - MRSA			35	24	5
CTEQ3M - MRSA			20	73	47
CTEQ2M - MRSA			16	48	6
CTEQ4M - MRSA			8	22	41

Table 5: Variation in extracted M_W and M_Z (in MeV) from central electron sample due to various sources, as obtained from [1].

Source	δM_Z (CC-CC)	δM_Z (CC-EC)	δM_W (m_t)	δM_W (p_t^e)	δM_W (p_t^ν)
CDC scale	-29	-33	-38	-40	-52
200 MeV EM offset	387	467	367	359	374
backgrounds			10	20	20
EM constant term c_{ecem}			23	14	27
α_{rec} hadronic response			-20	-16	46
hadronic resolution			25	10	90
$U_{\|\|}$ correction			15	15	20
$U_{\|\|}$ efficiency			2	-9	120
$r_0^{e\gamma}$	19	10	3	6	0
$P_T(W)$ spectrum			10	50	25
MRSD-' - MRSA			20	19	20
CTEQ3M - MRSA			5	48	22
CTEQ2M - MRSA			-21	-17	-30
CTEQ4M - MRSA			15	-5	13

Table 6: Contributions (in MeV) of the EC measurement uncertainties to the EC W mass result and the combined CC+EC result.

Source	m_t fit EC	m_t fit CC+EC
CC-EC Z mass stat. error	37	16
EC-EC Z mass stat. error	179	34
EC W stat. error	107	21
CC-EC Z width stat. error	47	14
EC-EC Z width stat. error	56	4
FDC radial scale	16	4
FDC-EC radial scale	23	6
ECEM offset	50	4
hadronic response	16	10
hadronic resolution	45	21
EC W background	21	4
PDF	35	15
$p_t(W)$	22	9
$\Gamma(W)$	10	6
radiative corrections	4	1

We therefore find the average EC EM scale relative to the Monte Carlo to be

$$\alpha_{ec} = 1.00001 \pm 0.00184 \tag{21}$$

Since the detector is north-south symmetric, and the liquid argon purity corrections have been applied to the data from each cryostat separately, we expect the observed EM scale in both EC's to be the same. Hence we have applied the same EM scale to both ECN and ECS. This is consistent with the W mass measurements given in equation 18

$$\begin{aligned}
M_W^{ECN} - M_W^{ECS} &= 33 \pm 210 \text{ MeV } (m_t \text{ fit}) \\
M_W^{ECN} - M_W^{ECS} &= -213 \pm 253 \text{ MeV } (p_t^e \text{ fit}) \\
M_W^{ECN} - M_W^{ECS} &= 15 \pm 319 \text{ MeV } (p_t^\nu \text{ fit})
\end{aligned} \tag{22}$$

17.2 W Mass Error Analysis

We identify the following parameters of relevance to the W mass measurement

- W mass statistical errors $\delta\omega_{cc}$ and $\delta\omega_{ec}$
- EM scales α_{cc} and α_{ec}
- EM offsets δ_{cc} and δ_{ec}
- FDC scale β_{fdc} and FDC-EC relative scale β_{ec}
- CDC scale β_{cdc}
- EM resolutions (constant terms) c_{ccem} and c_{ecem}
- recoil response α_{had}
- recoil resolution c_{had} representing jointly the sampling term s_{rec} and α_{mb}
- backgrounds b_{cc} and b_{ec}
- $U_{||}$ corrections u_{cc} and u_{ec}

- $U_{||}$ efficiencies ε_{cc} and ε_{ec}
- radiative corrections as a function of coalescing radius r_0
- theoretical modeling t

We take the EM scales, EM offsets, angular scales and the radiative correction to be a set of parameters that jointly determine the measured W and Z masses. We also take the EM resolution parameters as a correlated set. We take all the other parameters to be uncorrelated with them and with each other. We take the CC and EC backgrounds to be uncorrelated, and the the recoil modelling and the theoretical modelling (including PDF's, $p_T(W)$ spectrum and W width) to be common and therefore correlated.

The following measurements provide information on the values of these parameters

- The Z mass measurements M_Z^{cc-cc}, M_Z^{cc-ec} and M_Z^{ec-ec}
- FDC radial calibration θ_{fdc} and FDC-EC relative radial calibration θ_{ec}
- CDC z calibration θ_{cdc}
- CC and EC EM offsets δ_{cc} and δ_{ec}
- Gaussian width fitted to Z peak σ_Z^{cc-cc}, σ_Z^{cc-ec} and σ_Z^{ec-ec}
- p_t balance in Z events $\bar{p_t}$
- width of p_t balance in Z events σ_{pt}
- measurements of $U_{||}$ correction and $U_{||}$ efficiency
- constraints on theoretical model

We express the variations on the Z mass and width measurements as a linear combination of the variations on the parameters

$$\begin{aligned} \vec{\delta} M_Z &= \Delta_Z\, \vec{\delta} p \\ \vec{\delta} \sigma_Z &= \Delta_{\sigma_Z}\, \vec{\delta} c_{em} \end{aligned} \tag{23}$$

where $\vec{\delta} M_Z = (\delta M_Z^{cc-cc}, \delta M_Z^{cc-ec}, \delta M_Z^{ec-ec}, \delta\theta_{fdc}, \delta\theta_{ec}, \delta\theta_{cdc}, \delta\delta_{cc}, \delta\delta_{ec}, \delta r_0)$, $\vec{\delta} p = (\delta\alpha_{cc}, \delta\alpha_{ec}, \delta\beta_{fdc}, \delta\beta_{ec}, \delta\beta_{cdc}, \delta\delta_{cc}, \delta\delta_{ec}, \delta r_0)$, $\vec{\delta}\sigma_Z = (\delta\sigma_Z^{cc-cc}, \delta\sigma_Z^{cc-ec}, \delta\sigma_Z^{ec-ec})$

and $\vec{\delta}c_{em} = (\delta c_{ccem}, \delta c_{ecem})$. Δ represents the matrix of partial derivatives of the observables with respect to the parameters.

Similarly, the variations on the W mass are related linearly to the parameter variations

$$
\begin{aligned}
\vec{\delta}M_W &= \Delta_W\, \vec{\delta}p \\
&+ \Delta_{\sigma_W}\, \vec{\delta}c_{em} \\
&+ \Delta_{recoil\ scale}\, \delta\alpha_{had} \\
&+ \Delta_{recoil\ resolution}\, \delta c_{had} \\
&+ \Delta_{background}\, \vec{\delta}b \\
&+ \Delta_u\, \vec{\delta}u \\
&+ \Delta_\varepsilon\, \vec{\delta}\varepsilon \\
&+ \Delta_{theory}\, \delta t \\
&+ \vec{\delta}\omega_W
\end{aligned}
\tag{24}
$$

where $\vec{\delta}M_W = (\delta M_W^{cc}, \delta M_W^{ec})$.

Using generalized least squares fitting, and assuming that the errors on the components of $\vec{\delta}M_Z$ and $\vec{\delta}\sigma_Z$ are uncorrelated, we fit for the parameter vectors $\vec{p}$ and $\vec{\delta}c_{em}$. The fit also produces the covariance matrix on these parameters. We then propagate the parameter covariance matrices into the covariance matrix on the CC and EC W mass measurements using equation 24, by identifying the latter with the expected value of $\vec{\delta}M_W(\vec{\delta}M_W)^T$, where ^{T} indicates the transpose. The various contributions to $\vec{\delta}M_W$ are independent, hence they contribute additively to the total covariance matrix. Using the covariance matrix , we get the following results for the transverse mass fit

$$
\begin{aligned}
M_W &= 80.766 \pm 0.234 \text{ GeV (EC)} \\
M_W &= 80.497 \pm 0.098 \text{ GeV (CC \& EC combined)}
\end{aligned}
\tag{25}
$$

where the published [1] CC results are used in the combination. The χ^2 for the CC-EC combination is 1.6 for one degree of freedom, with a probability of 21%.

Combining with the Run 1A measurement according to equations 57 and 58 of [1] and taking 50 MeV as common error between the Run 1A and the

Run 1B measurements (table XIV of [1]), we obtain the Run 1 measurement from the transverse mass fit

$$M_W = 80.483 \pm 0.094 \text{ GeV} \tag{26}$$

Using the technique described above, we can also combine the CC and EC results for the $p_t(e)$ and $p_t(\nu)$ fits. For the $p_t(e)$ fit, we obtain

$$\begin{aligned} M_W &= 80.587 \pm 0.250 \text{ GeV (EC)} \\ M_W &= 80.497 \pm 0.123 \text{ GeV (CC \& EC combined)} \end{aligned} \tag{27}$$

The χ^2 is 0.17 with a probability of 68%.

For the $p_t(\nu)$ fit we obtain

$$\begin{aligned} M_W &= 80.726 \pm 0.347 \text{ GeV (EC)} \\ M_W &= 80.405 \pm 0.168 \text{ GeV (CC \& EC combined)} \end{aligned} \tag{28}$$

The χ^2 is 1.1 with a probability of 29%.

We can also combine all the six measurements (CC and EC fits with the three techniques). We obtain the combined run 1b measurement

$$M_W = 80.487 \pm 0.096 \text{ GeV (CC \& EC combined)} \tag{29}$$

The χ^2 is 4.6/5 dof, with a probability of 46%. Combining with the run 1a measurement gives the run 1 measurement:

$$M_W = 80.474 \pm 0.093 \text{ GeV} \tag{30}$$

References

[1] *A Measurement of the W Boson Mass,* Phys. Rev. D58, 092003 (1998); DØ note 3198, *W Boson Mass Measurement,* I. Adam, E. Flattum, U. Heintz, April 1997.

[2] *Determination of the Mass of the W Boson using the DØ Detector at the Tevatron,* Phys. Rev. D58, 012002 (1998); DØ note 2929, *Measurement of the W Mass,* Marcel Demarteau, John Sculli, Kathleen Streets, April 1996.

[3] Ian Adam, Ph.D. thesis, Columbia University, 1997.

[4] Eric Flattum, Ph. D. thesis, Michigan State University, 1996.

[5] DØ note 3232, *Transverse Alignment of Forward Drift Chambers using Electrons,* Ashutosh V. Kotwal, May 1997.

[6] DØ note 3234, *Axial Calibration of the DØ Central Drift Chamber,* Run 1 Central Detector Tracking Analysis Group.

[7] DØ note 3328, *Relative Transverse Alignment of Endcap Calorimeters and Forward Drift Chambers using Electrons,* Ashutosh V. Kotwal, October 1997.

[8] DØ note 3341, *Relative Radial Position Calibration of Endcap Calorimeters and Forward Drift Chambers using $Z \rightarrow ee$ Events,* Ashutosh V. Kotwal, October 1997.

[9] DØ note 3404, *Underlying Event Contribution to Electron Energy and Recoil Correction in Endcap Calorimeters,* Ashutosh V. Kotwal, February 1998.

[10] DØ note 3395, *Measurement of the Run 1b Electron Trigger Turnon for the Endcap Calorimeters,* J. Andrew Green, Ashutosh V. Kotwal, February 1998.

[11] DØ note 3392, *QCD Background in the $W \rightarrow e\nu$ Sample at Low p_t^W in Endcap Calorimeters,* Ashutosh V. Kotwal, February 1998.

[12] Dylan Casey, Private Communication.

[13] DØ note 3608, *Determination of Electromagnetic Energy Offset for EC Electrons in DØ Detector,* Yaroslav Kulik, February 1999.

[14] Ron Madaras, private communication.

[15] DØ note 3607, *Determination of the $U_{||}$ Efficiency for EC Electrons for W Mass Analysis,* Yaroslav Kulik, February 1999.

[16] Using CMS Monte Carlo code v4.5 and rcp v3440.

[17] DØ note 3233, *Radial Calibration of Forward Drift Chambers using Collider Muons,* Ashutosh V. Kotwal, June 1997.